Improving power-grid systems via topological changes or how self-organized criticality can help power grids

Géza Ódor, S. Deng, I. Papp, K. Benedek and B. Hartmann
Centre for Energy Research, Budapest,
Jeffery Kelling TU. Chemnitz and HZDR, Dresden

Strategic research area project of ELKH

TECHNISCHE UNIVERSITÄT IN DER KULTURHAUPTSTADT EUROPAS CHEMNITZ

HUN REN Energiatudományi Kutatóközpont

Nemzeti Kutatási, Fejlesztési és Innovációs Hivatal

Dynamic Days 2024

Géza Ódor, István Papp, Kristóf Benedek, and Bálint Hartmann
Phys. Rev. Research 6, (2024) 013194, Smart E. and Grids 2024

Large-scale blackouts in the world and their consequences

No.	Country	Year	Load loss (GW)	Economic loss	People affected (*Million)	Duration (hours)	Reference
1	Iran	2003	~7	Not available	22	8	[10, 13]
2	USA, Canada	2003	61.8	$ 6.4 billion	50	16–72 (USA), up to 192 (Canada)	[10-12]
3	Italy	2003	24	Over €120 million	~56	Up to ~18	[10, 12]
4	Russia	2005	~3.5	$ 1–2 billion	4	~4	[46, 50]
5	Western Europe	2006	~14	Not available	15	~2	[12]
6	USA and Mexico	2011	4.3	Up to $118 million	Over 5	~11	[50]
7	India	2012	~48	Not available	670	2–8	[13, 51]
8	Turkey	2015	32.2	Not available	70	More than 7	[13]

Large-scale blackouts in the world and their consequences

No.	Country	Year	Load loss (GW)	Economic loss	People affected (*Million)	Duration (hours)	Reference
1	Iran	2003	~7	Not available	22	8	[10, 13]
2	USA, Canada	2003	61.8	$ 6.4 billion	50	16–72 (USA), up to 192 (Canada)	[10-12]
3	Italy	2003	24	Over €120 million	~56	Up to ~18	[10, 12]
4	Russia	2005	~3.5	$ 1–2 billion	4	~4	[46, 50]
5	Western Europe	2006	~14	Not available	15	~2	[12]
6	USA and Mexico	2011	4.3	Up to $118 million	Over 5	~11	[50]
7	India	2012	~48	Not available	670	2–8	[13, 51]
8	Turkey	2015	32.2	Not available	70	More than 7	[13]

Renewable energy adds more instability due to the large fluctuations of the power sources, like wind farms:

Anvari et al 2018
Complexity and Synergetics.

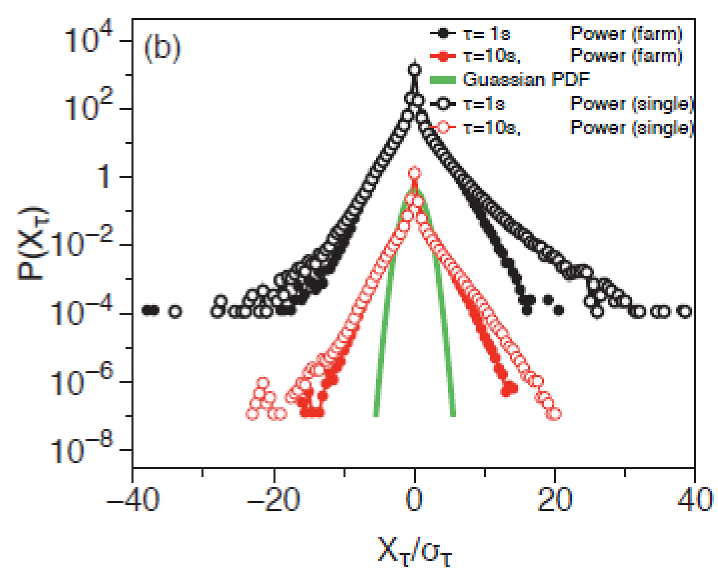

Scale-free blackout size distributions

Scale-free blackout size distributions

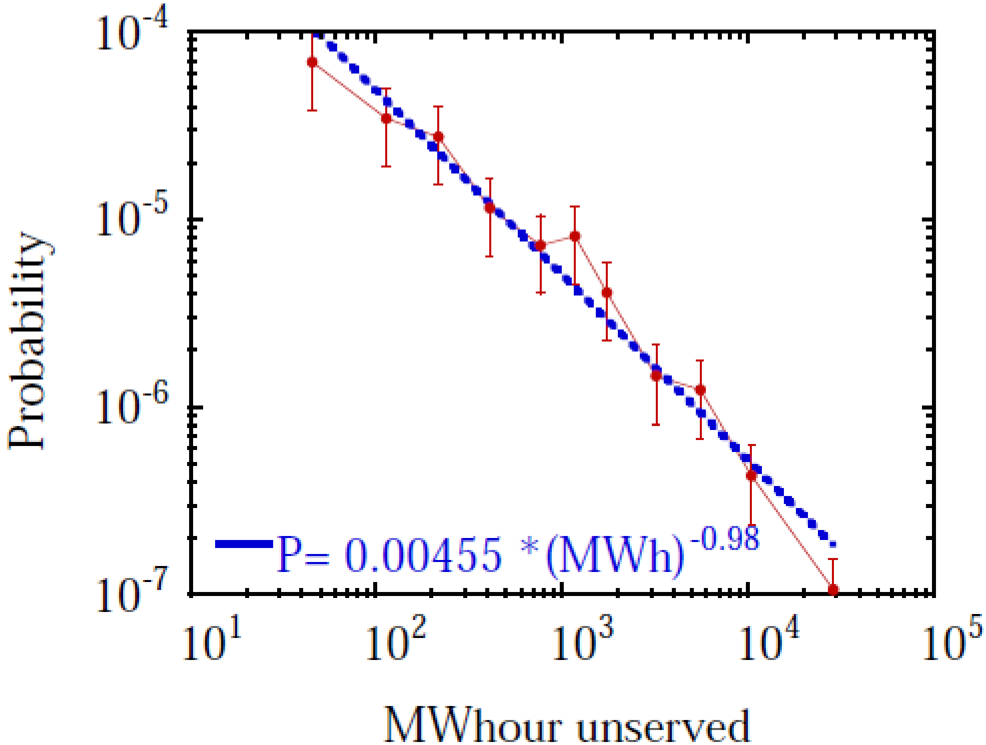

Figure 4. Probability distribution function of energy unserved for North American blackouts 1993-1998.

B. Carreras et al, Proceedings of Hawaii International Conference on System Sciences, Jan. 4-7, 2000, Maui, Hawaii. 2000 IEEE

Scale-free blackout size distributions

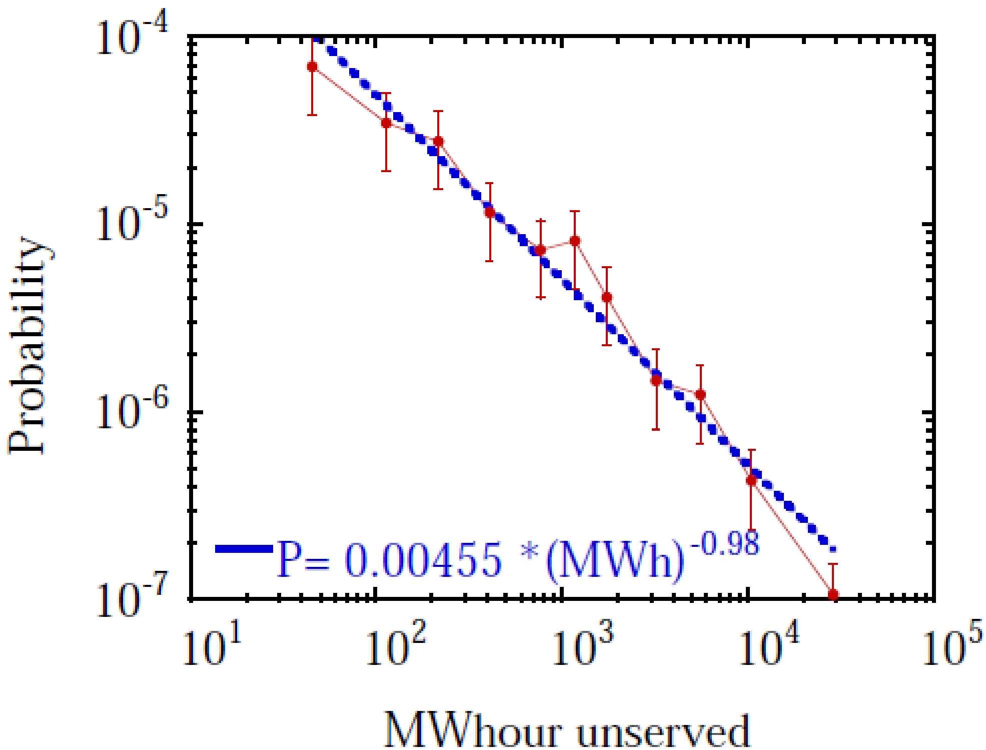

Figure 4. Probability distribution function of energy unserved for North American blackouts 1993-1998.

B. Carreras et al, Proceedings of Hawaii International Conference on System Sciences, Jan. 4-7, 2000, Maui, Hawaii. 2000 IEEE

Extreme events occur more frequently than by an independent variable ensemble

Scale-free blackout size distributions

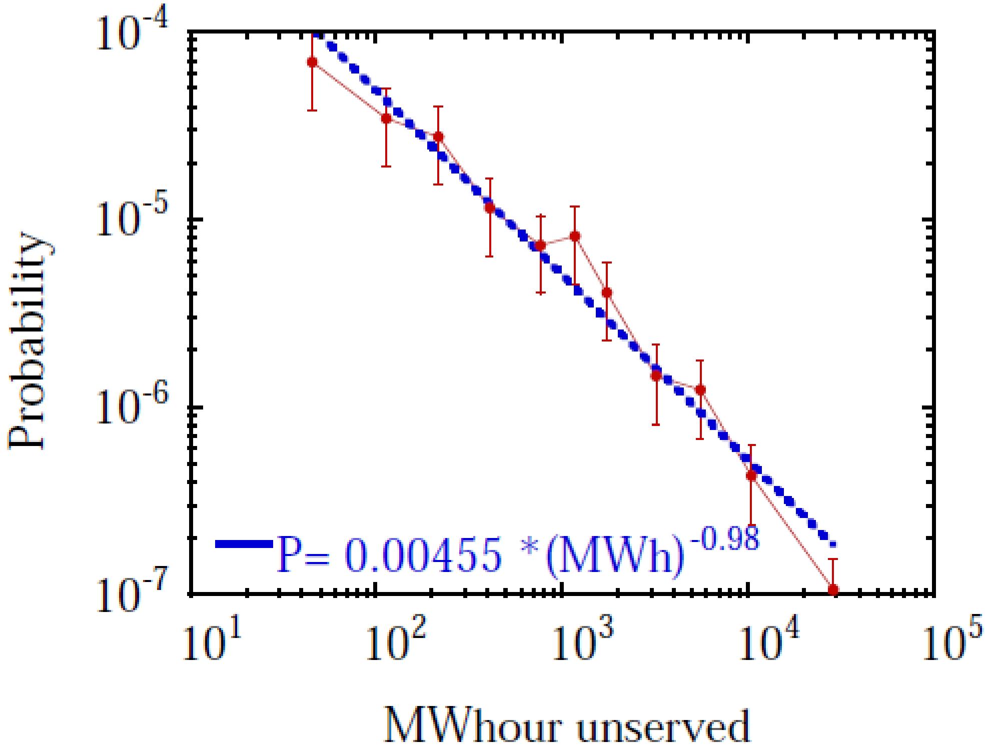

Figure 4. Probability distribution function of energy unserved for North American blackouts 1993-1998.

B. Carreras et al, Proceedings of Hawaii International Conference on System Sciences, Jan. 4-7, 2000, Maui, Hawaii. 2000 IEEE

Extreme events occur more frequently than by an independent variable ensemble

Self-Organized Criticality (SOC) was assumed to describe this:

Competition of supply and demand

Scale-free blackout size distributions

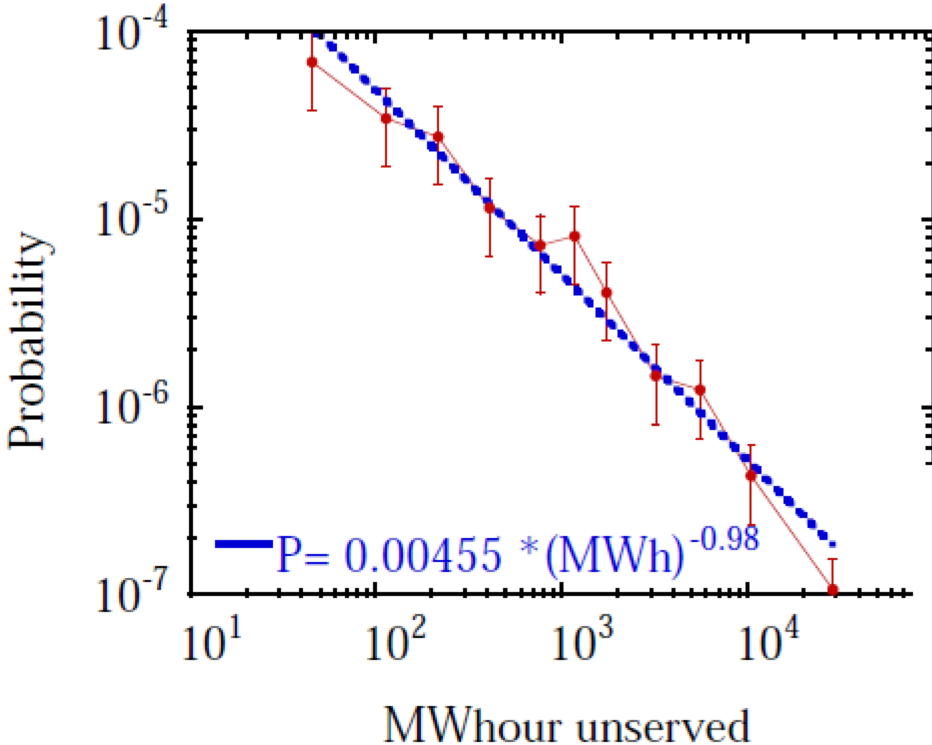

Figure 4. Probability distribution function of energy unserved for North American blackouts 1993-1998.

B. Carreras et al, Proceedings of Hawaii International Conference on System Sciences, Jan. 4-7, 2000, Maui, Hawaii. 2000 IEEE

Extreme events occur more frequently than by an independent variable ensemble

TABLE I. Observed and simulated power law exponents in the noncumulative pdf of blackout size. The power law exponent is often calculated by subtracting one from an estimate of the slope of a log-log plot of a complementary cumulative probability distribution.

Source	Exponent	Quantity
North America data (Ref. 6)	−1.3 to −2.0	Various
North America data (Refs. 19 and 20)	−2.0	Power
Sweden data (Ref. 21)	−1.6	Energy
Norway data (Ref. 22)	−1.7	Power
New Zealand data (Ref. 23)	−1.6	Energy
China data (Ref. 24)	−1.8	Energy
	−1.9	Power
OPA model on tree-like 382-node (Ref. 8)	−1.6	Power
Hidden failure model on WSCC 179-node (Ref. 9)	−1.6	Power
Manchester model on 1000-node (Ref. 10)	−1.5	Energy
CASCADE model (Ref. 11)	−1.4	No. of failures
Branching process model (Ref. 12)	−1.5	No. of failures

Dobson et al Chaos 17 (2007) 026103

Self-Organized Criticality (SOC) was assumed to describe this:

Competition of supply and demand

The EU 2016 HV network

SciGRID project based on ENTSO-E & OpenStreetMap data

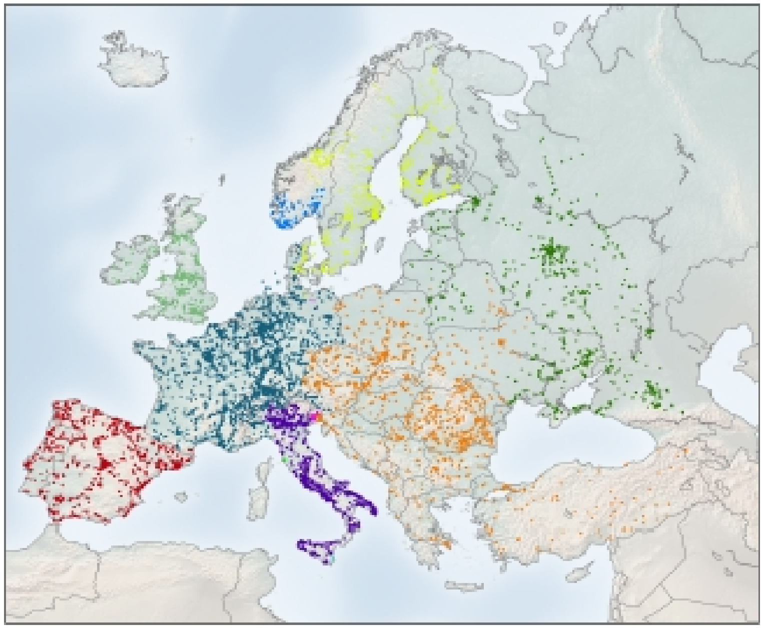

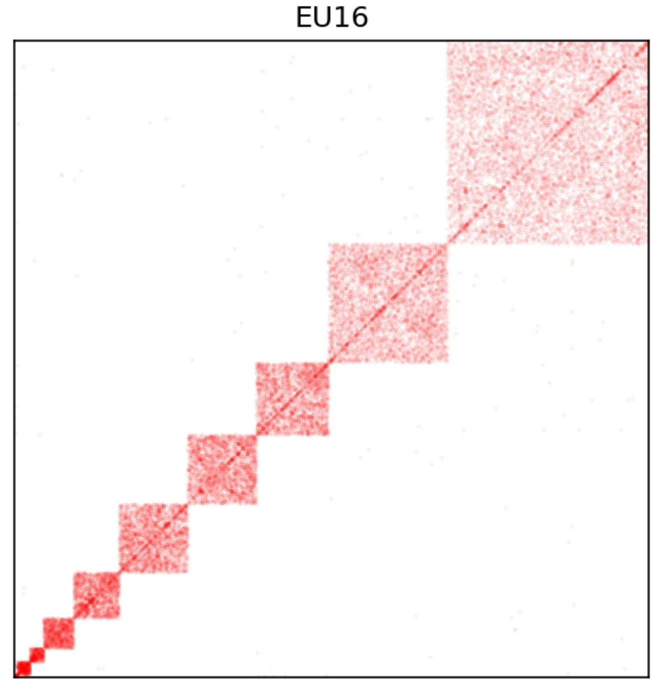

FIG. 9. All nodes of the European power-grid 2016 data separated into 12 communities, taking into account admittance using a giant component of 13 478 nodes connected by 18 39[illegible] links, maintaining the modularity score close to the maximum $Q \approx 0.795$.

Adjacency Matrix

Graph dimension: $\langle N_r \rangle \sim r^d,$

The EU 2016 HV network

SciGRID project based on ENTSO-E & OpenStreetMap data

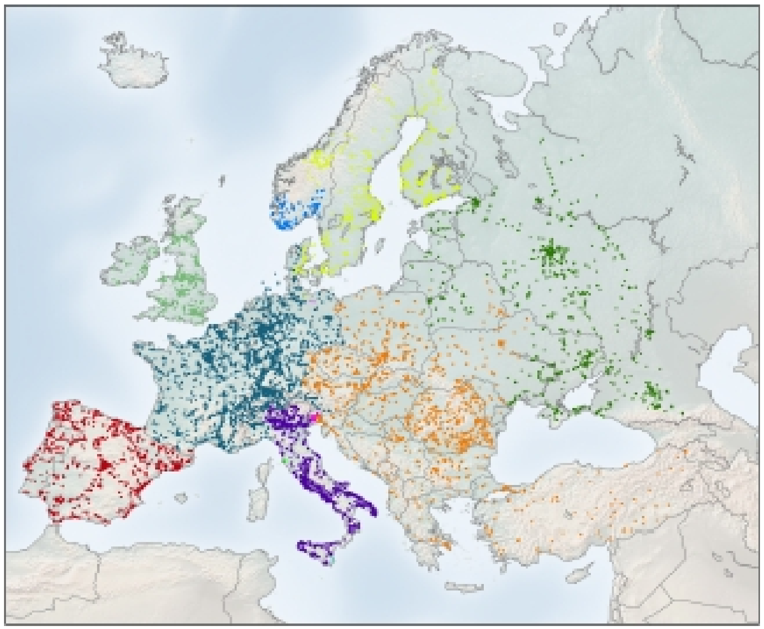

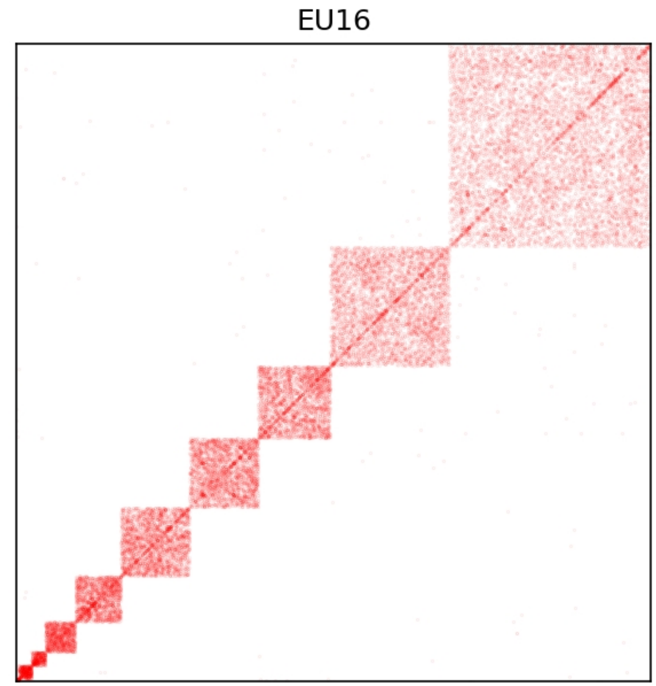

FIG. 9. All nodes of the European power-grid 2016 data sep-
arated into 12 communities, taking into account admittance
using a giant component of 13 478 nodes connected by 18 39:
links, maintaining the modularity score close to the maximun
$Q \approx 0.795$.

Adjacency Matrix

Graph dimension: $\langle N_r \rangle \sim r^d,$

Modular HV network, with graph dimension d = $2.6(1)$, but $d_s < 2$

The US 2016 HV network

SciGRID project based on ENTSO-E & OpenStreetMap data

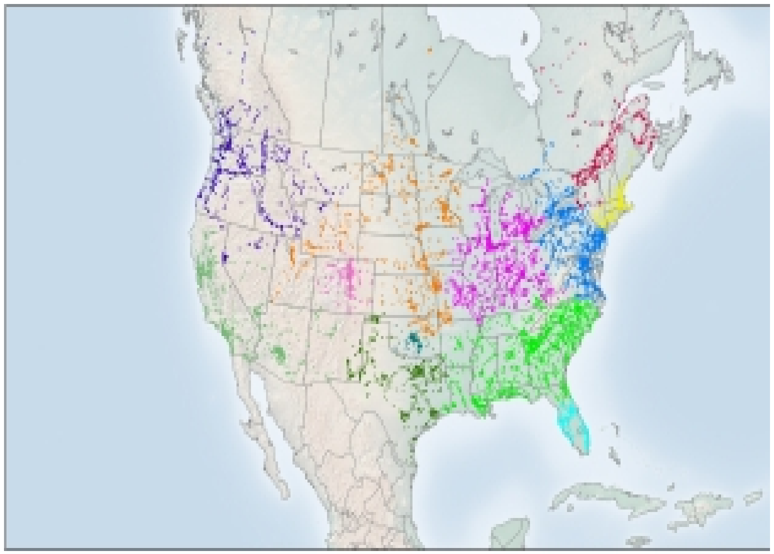

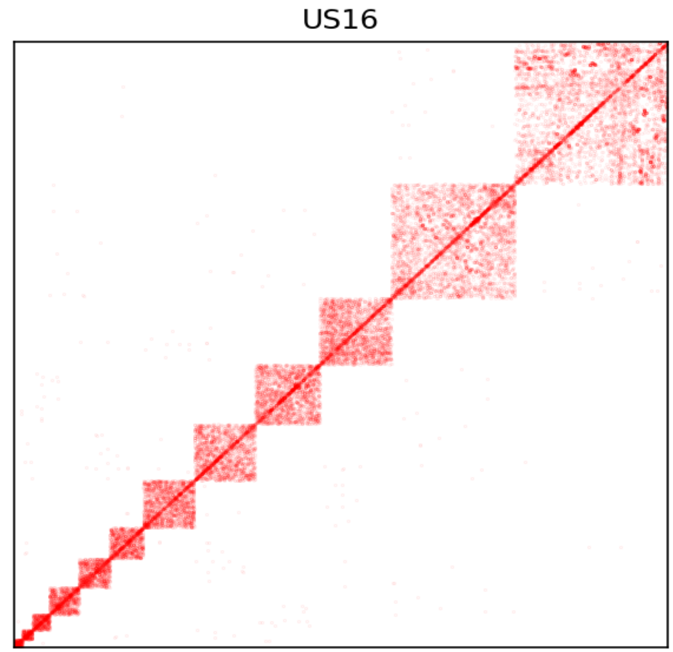

FIG. 12. All nodes of the USA power-grid 2016 data giant component, separated into 12 communities, taking into account the admittances and 14 990 nodes connected by 20 880 edges, maintaining the modularity score $Q \approx 0.859$ with resolution $\Gamma = 1 \times 10^{-4}$.

Adjacency Matrix

The US 2016 HV network

SciGRID project based on ENTSO-E & OpenStreetMap data

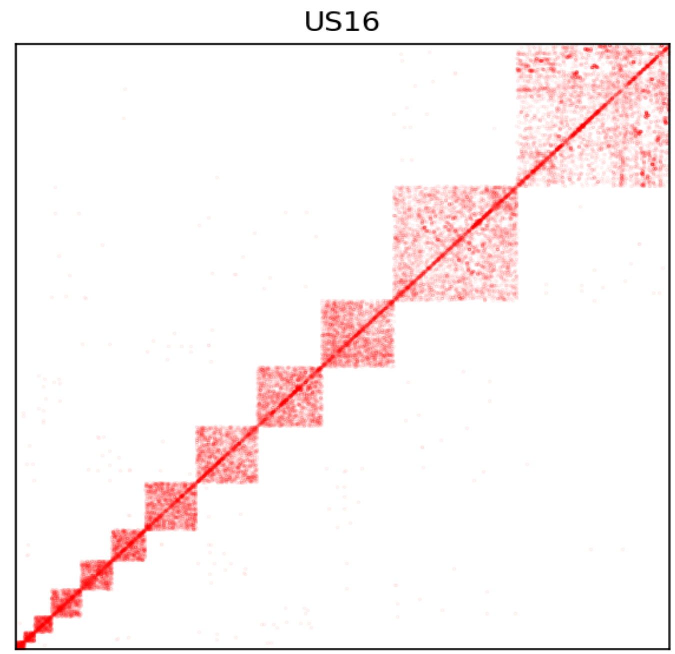

FIG. 12. All nodes of the USA power-grid 2016 data giant component, separated into 12 communities, taking into account the admittances and 14 990 nodes connected by 20 880 edges, maintaining the modularity score $Q \approx 0.859$ with resolution $\Gamma = 1 \times 10^{-4}$.

Adjacency Matrix

Modular HV network, with with graph dimension d = *2.4(1)*

The EU 2022 HV network

SciGRID project based on ENTSO-E & OpenStreetMap data

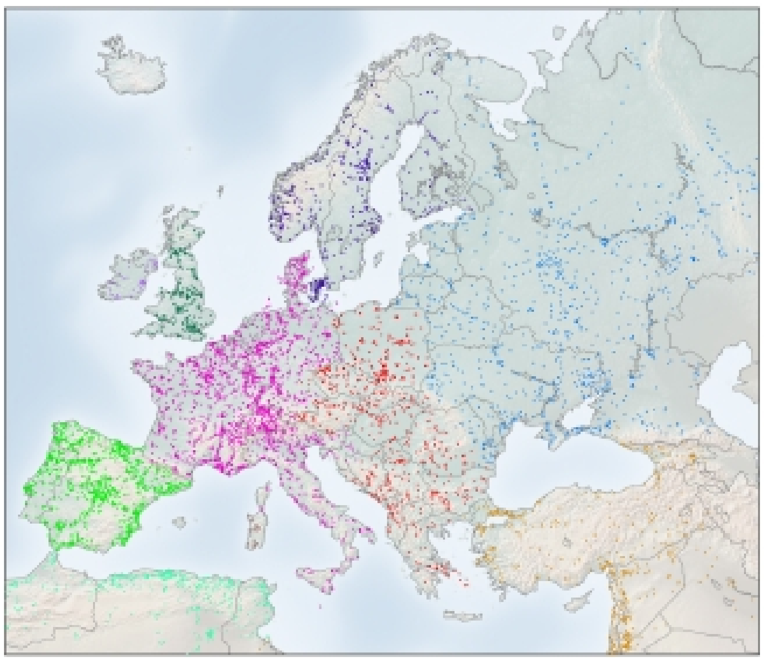

FIG. 11. All nodes of the European power-grid 2022 data giant component, separated into 10 communities, taking into account the admittances and 7411 nodes connected by 10 912 edges without smaller voltage level edges, maintaining the modularity score $Q \approx 0.854$.

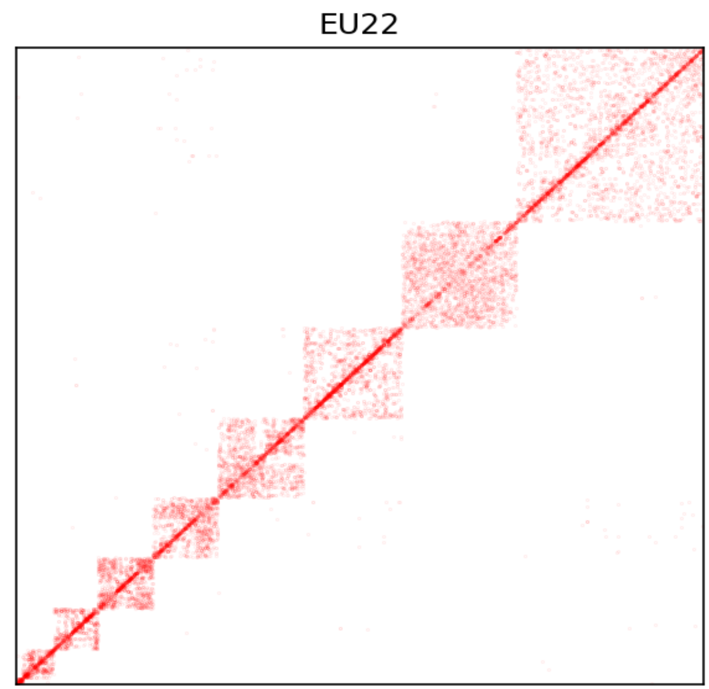

Adjacency Matrix

The EU 2022 HV network

SciGRID project based on ENTSO-E & OpenStreetMap data

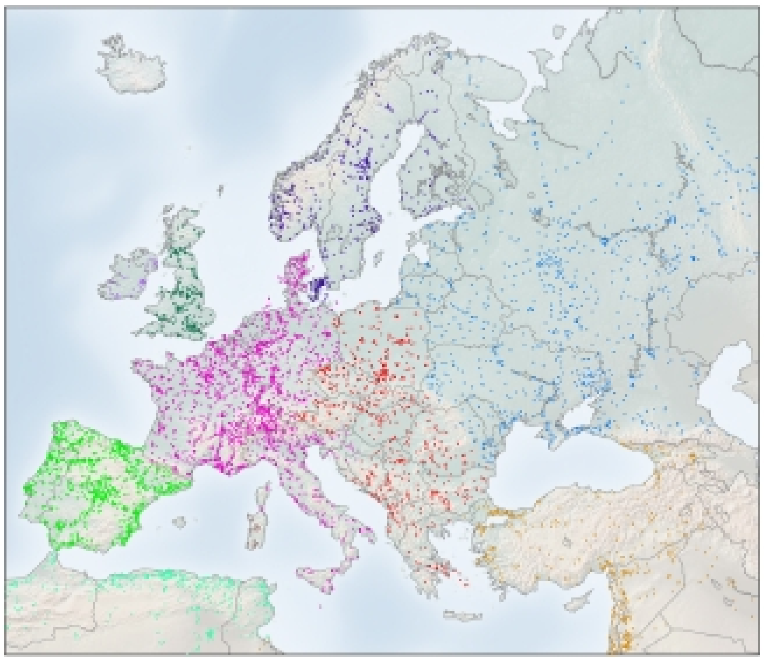

FIG. 11. All nodes of the European power-grid 2022 data giant component, separated into 10 communities, taking into account the admittances and 7411 nodes connected by 10 912 edges without smaller voltage level edges, maintaining the modularity score $Q \approx 0.854$.

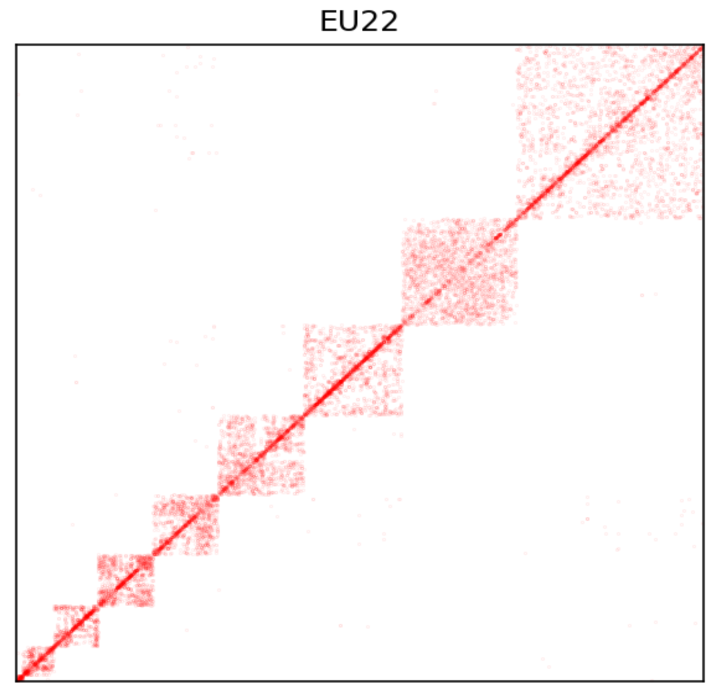

Adjacency Matrix

Modular HV network, with graph dimension: d = *1.8(2)*

Incomplete network

Summary of network invariants

Graph: $G = (V, E)$ *N* nodes, *E* edges

Average degree $\langle k \rangle = \frac{1}{N} \sum_{i=1}^{N} k_i$

Cumulative degree distribution $P(k_i > K) = C \cdot e^{-\frac{k_i}{\gamma_c}}$

Shortest path-length $L = \frac{1}{N(N-1)} \sum_{j \neq i} d(i,j)$, $L_r = \frac{\ln N - 0,5772}{\ln \langle k \rangle} + 1/2$

Clustering coefficient $C = \frac{1}{N} \sum_i 2n_i / k_i (k_i - 1)$

Small world coefficient $\sigma = \frac{C/C_r}{L/L_r}$ Modularity $Q = \frac{1}{N\langle k \rangle} \sum_{ij} \left(A_{ij} - \Gamma \frac{k_i k_j}{N \langle k \rangle} \right) \delta(g_i, g_j)$

Network	E	N	$\langle k \rangle$	γ_c	Q	Community #	L	L_r	C	C_r	σ
EU16	18393	13478	2,729	1,504	0,924	28	49,50	9,396	0,099	0,000203	92,702
EU22	10298	7411	2,779	1,640	0,849	12	46,83	8,653	0,098	0,000375	48,420
USA16	20880	14990	2,786	1,548	0,927	22	47,50	9,321	0,102	0,000186	107,785

Similar invariants, small world networks, but *d* < *3*

The synchronization model

- Blackouts can be modeled by desynchronization of AC power grids
- Power transmission: a mismatch "$\Delta\theta$" in the phases between "G" and "M" $\Rightarrow$ the Kuramoto model with **inertia** [1]:

$$
\begin{aligned}
P_{\text{source}} &= P_{\text{acc.kinetic}} + P_{\text{diss.}} + P_{\text{transmitted}} \\
&= \frac{1}{2} I \frac{d}{dt} \dot{\theta}_1^2 + P_{\text{diss.}} - P^{\text{MAX}} \sin(\Delta\theta) \\
\Rightarrow \ddot{\theta}_1 &= P - \alpha\dot{\theta}_1 + P^{\text{MAX}} \sin(\Delta\theta).
\end{aligned}
\qquad (1)
$$

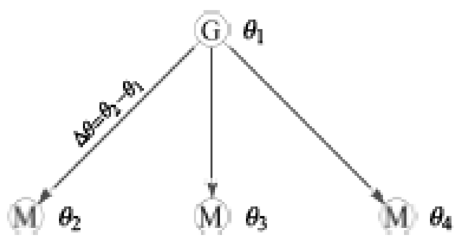

- For a network of N oscillators:

$$
\begin{aligned}
\dot{\theta}_i(t) &= \omega_i(t) \\
\dot{\omega}_i(t) &= \omega_i(0) - \alpha\dot{\theta}_i(t) + K \sum_{j=1}^{N} A_{ij} \sin\left[\theta_j(t) - \theta_i(t)\right] .
\end{aligned}
\qquad (2)
$$

α: damping factor; K: global coupling; $\omega_i(0) \sim N(0,1)$

[1] G. Filatrella *et al.*, Eur. Phys. J. B, **61**, 485–491 (2008).

Methods and measured quantities

- For large N, solved Eqs. (2) by numeric solvers: 4th-order Runge-Kutta, Bulirsch-Stoer
- For large K: adaptive **Bulirsch-Stoer**
- GPU code (kuramotoGPU) by utilizing VexCL's vector capability.

- Measured quantities
  1. Phase order parameter

$$z(t_k) = \frac{1}{N}\left|\sum_j \exp\left[i\theta_j(t_k)\right]\right|$$
$$R(t_k) = \langle r(t_k)\rangle \, . \qquad (3)$$

  2. Frequency variance: $\Omega(t_k) = \langle \mathrm{var}(\omega_i(t_k))\rangle$.

---

[1] H. Hong *et al.*, Phys. Rev. E, **72**, 036217 (2005).
[2] G. Ódor and B. Hartmann. Phys. Rev. E, **98** 022305 (2018).

Cascade simulations by line-cuts

After thermalization, randomly remove a link w.r.t. the overload condition:

$$|\sin(\theta_j - \theta_i)| > T \Rightarrow A_{ij} := 0.$$

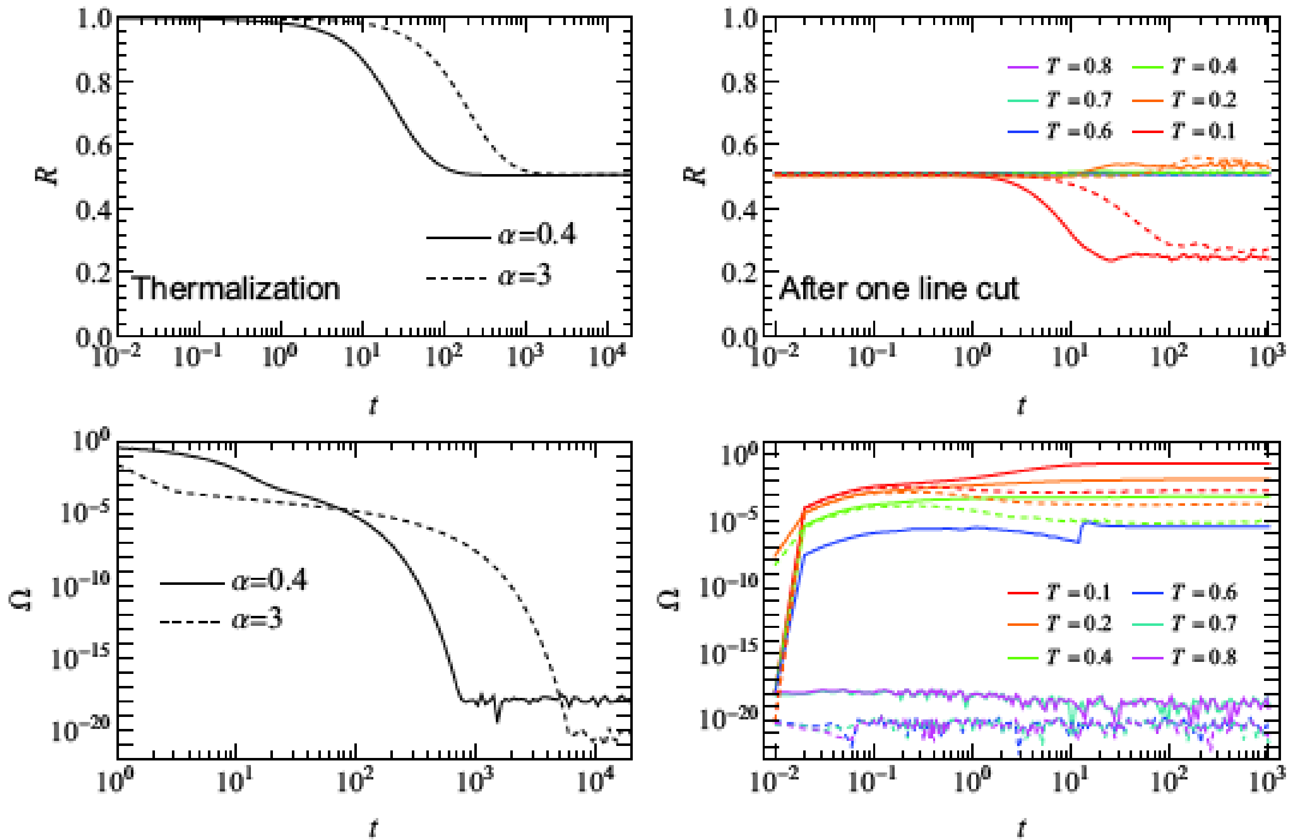

EU network $K = 80$

1. Stronger damping effect only slows down R, but leads to a smaller Ω.
2. For certain T, R may even increase: islanding effects?

Cascade failure statistics

US HV $K = 30, \alpha = 0.4$

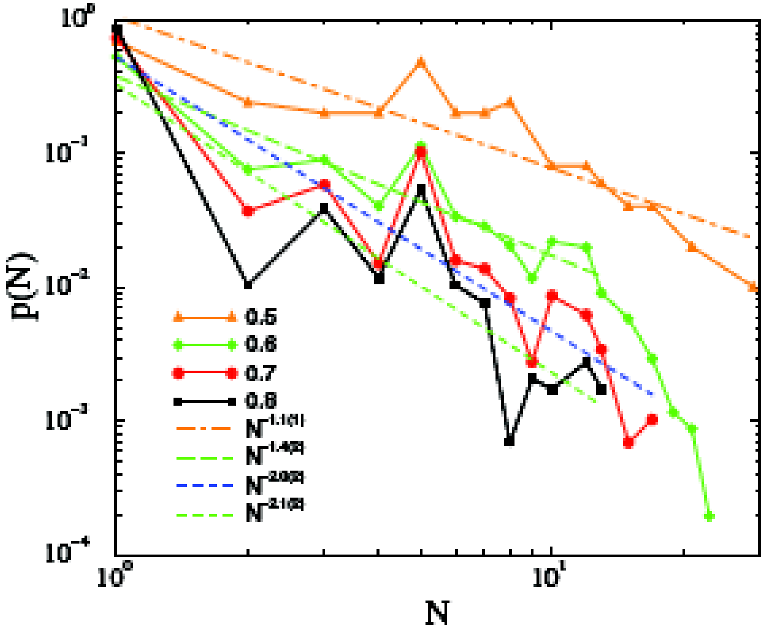

EU HV $K = 60, \alpha = 0.4$

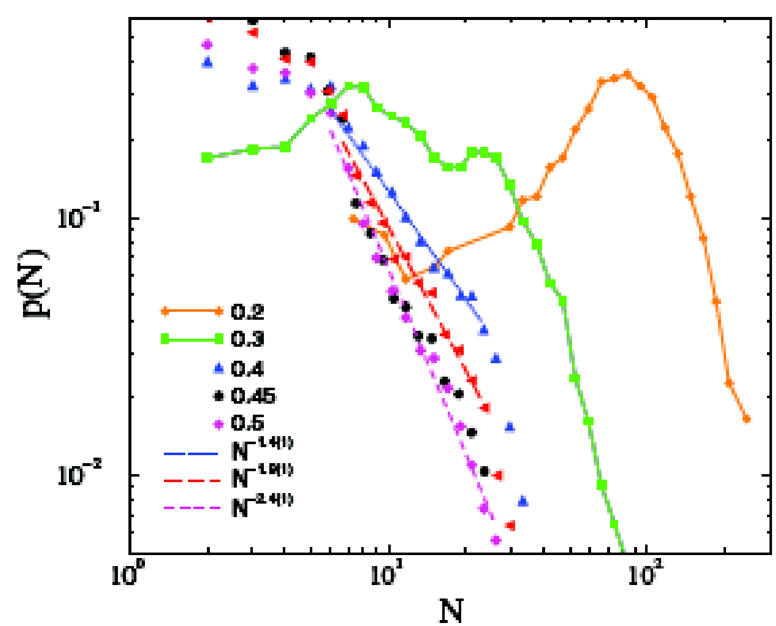

- The distribution of the total line failures N_f follows non-universal power laws in the vicinity of (K_c, T_c)

$$p(N_f) \sim N_f^{-\tau}.$$

Cascade failure statistics

US HV $K = 30, \alpha = 0.4$

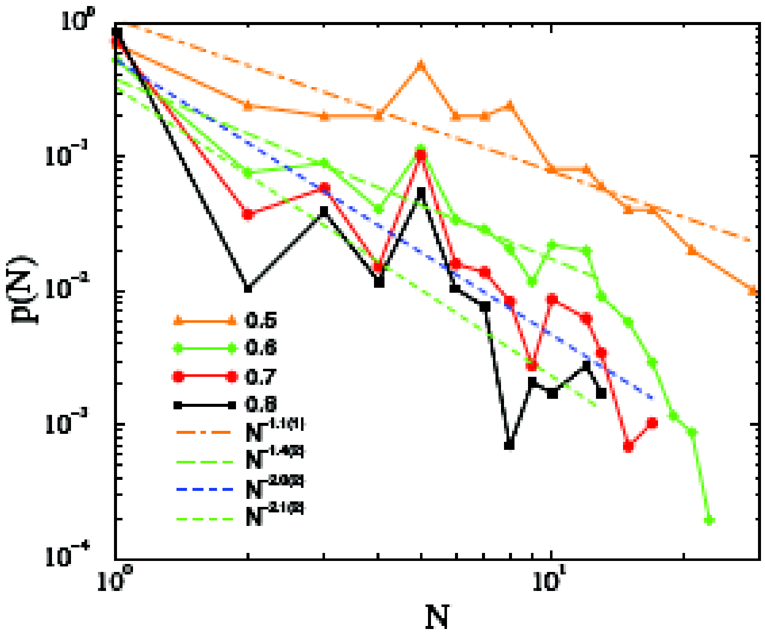

EU HV $K = 60, \alpha = 0.4$

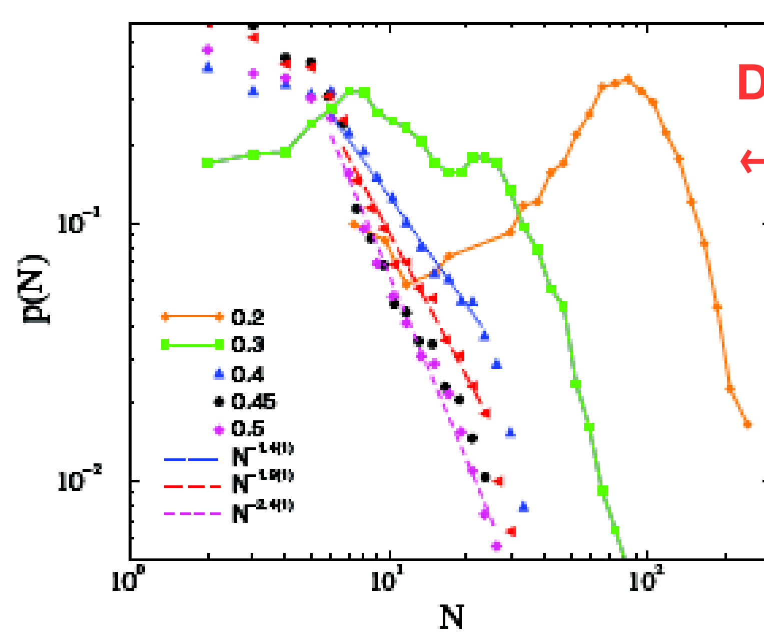

Dragon king

← events

- The distribution of the total line failures N_f follows non-universal power laws in the vicinity of (K_c, T_c)

$$p(N_f) \sim N_f^{-\tau}.$$

Fluctuation peaks and Island effects

Fluctuation peaks and Island effects

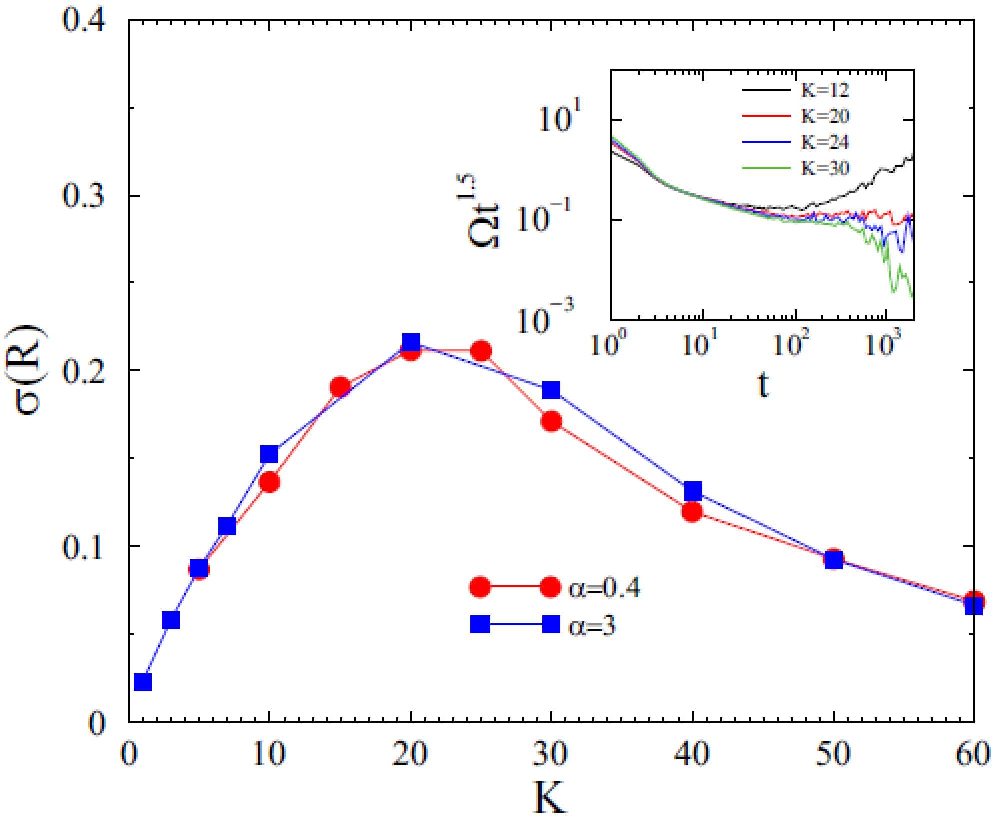

FIG. 9. Fluctuations of $R(t \to \infty)$ in case of the U.S.-HV power grid at the end of the thermalization process. Both for the normal $\alpha = 0.4$ and the $\alpha = 3$ dissipation cases. Partial synchronization transition occurs at $K_c \simeq 22(2)$. The inset shows the decay of $\Omega(t)$ starting from disordered states at $\alpha = 3$ and for different global couplings, as shown by the legends. The curves are multiplied by a factor $t^{1.5}$ in order to see the scaling at $K_c = 20$.

Fluctuation peaks and Island effects

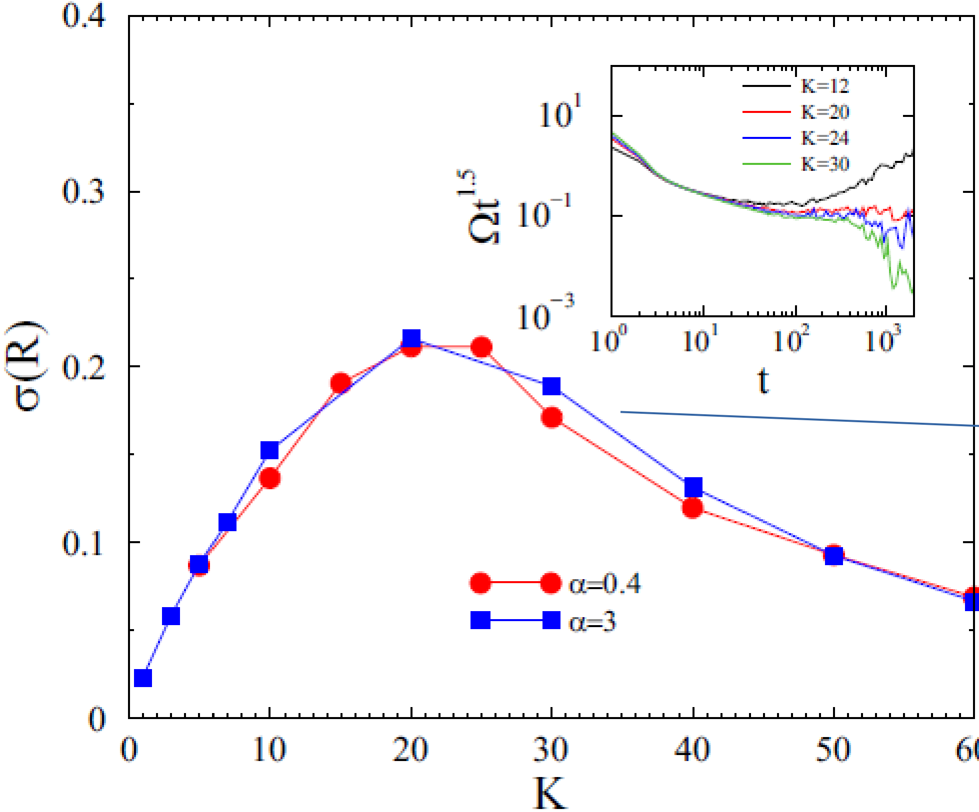

FIG. 9. Fluctuations of $R(t \to \infty)$ in case of the U.S.-HV powe grid at the end of the thermalization process. Both for the norma $\alpha = 0.4$ and the $\alpha = 3$ dissipation cases. Partial synchronizatio transition occurs at $K_c \simeq 22(2)$. The inset shows the decay of $\Omega(t$ starting from disordered states at $\alpha = 3$ and for different globa couplings, as shown by the legends. The curves are multiplied b a factor $t^{1.5}$ in order to see the scaling at $K_c = 20$.

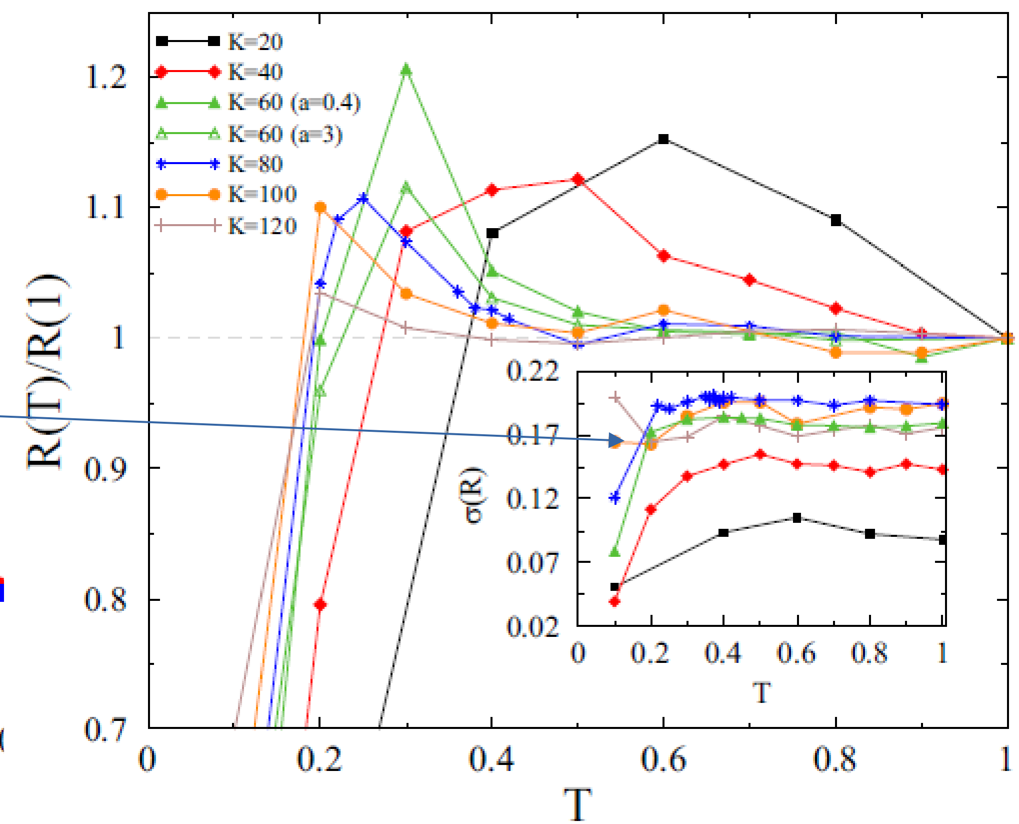

FIG. 16. Relative change of the steady-state Kuramoto order parameter at $\alpha = 0.4$ the consequence of the cascade in the Europe-HV grid. The $R(T = 1)$ values are set to be the reference points and $R(T)/R(T = 1)$ is plotted. The gray dashed line marks the baseline for the emergence of islanding effects. The inset shows $\sigma[R(T, K)]$.

Fluctuation peaks and Island effects

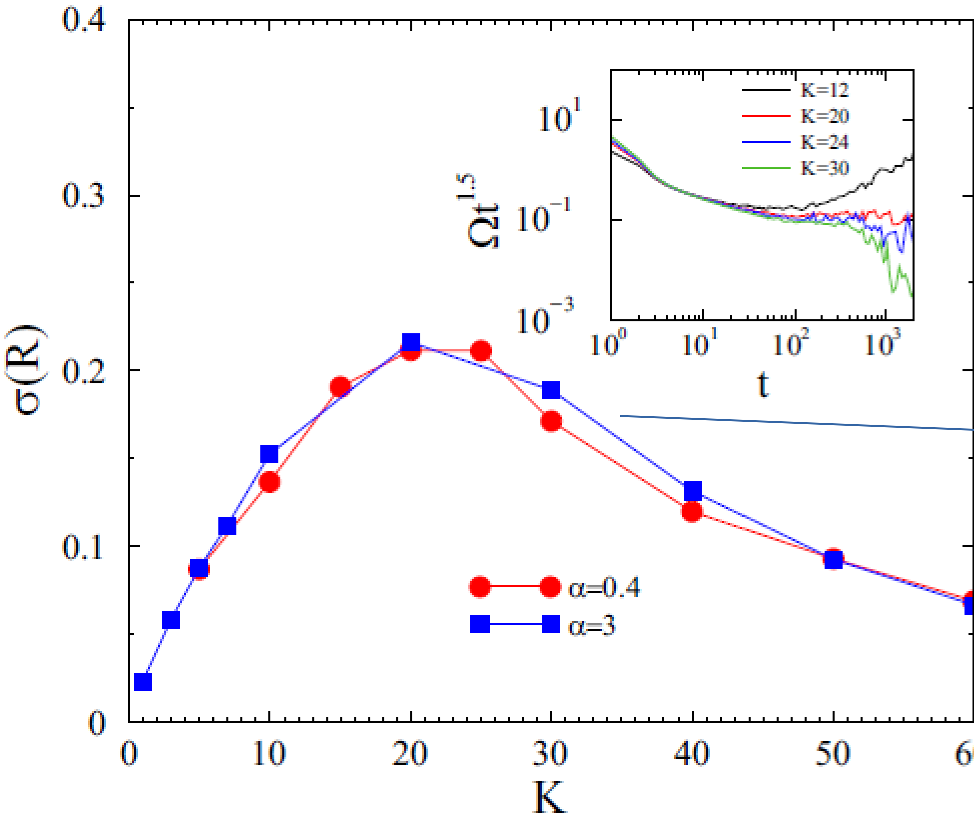

FIG. 9. Fluctuations of $R(t \to \infty)$ in case of the U.S.-HV powe grid at the end of the thermalization process. Both for the norma $\alpha = 0.4$ and the $\alpha = 3$ dissipation cases. Partial synchronizatio transition occurs at $K_c \simeq 22(2)$. The inset shows the decay of $\Omega(t$ starting from disordered states at $\alpha = 3$ and for different globa couplings, as shown by the legends. The curves are multiplied by a factor $t^{1.5}$ in order to see the scaling at $K_c = 20$.

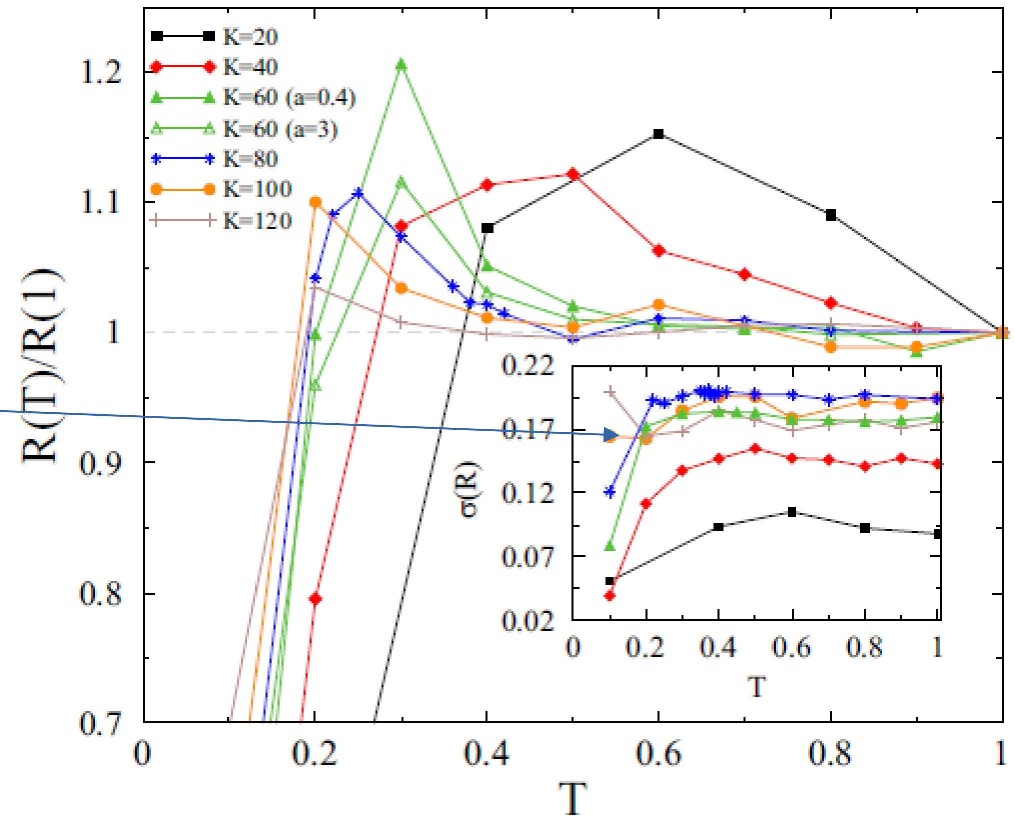

FIG. 16. Relative change of the steady-state Kuramoto order parameter at $\alpha = 0.4$ the consequence of the cascade in the Europe-HV grid. The $R(T = 1)$ values are set to be the reference points and $R(T)/R(T = 1)$ is plotted. The gray dashed line marks the baseline for the emergence of islanding effects. The inset shows $\sigma[R(T, K)]$.

Enhanced stability at *σ(R) peaks* , near the synchronization transition !

Comparison of frequency results with measurements of Hungarian HV power-grid

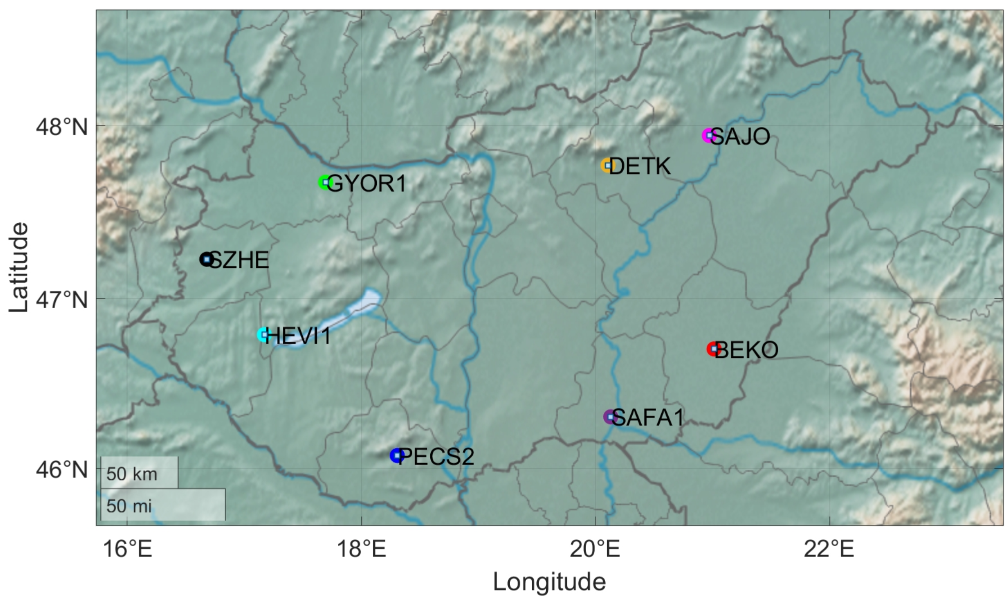

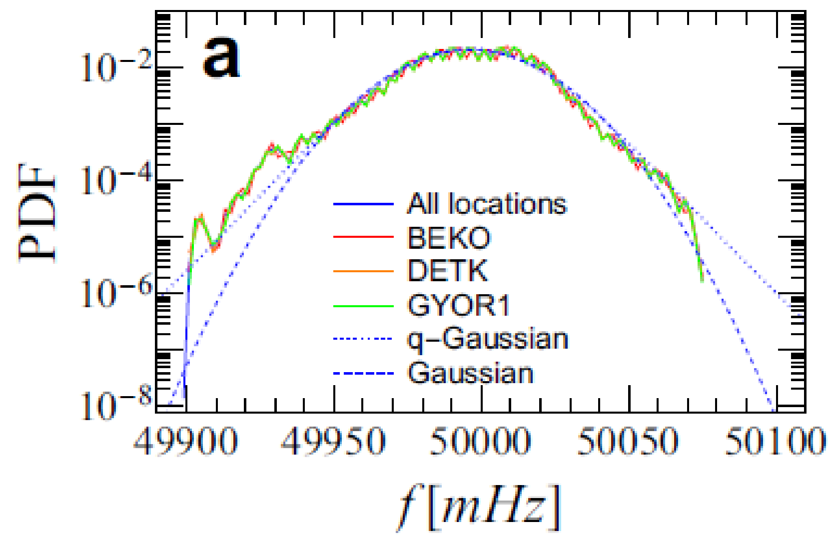

Frequency data in Hungary at 10/23 2022

Fits well with q-Gaussian *(q~1.1)* (*SEGAN*)

Comparison of frequency results with measurements of Hungarian HV power-grid

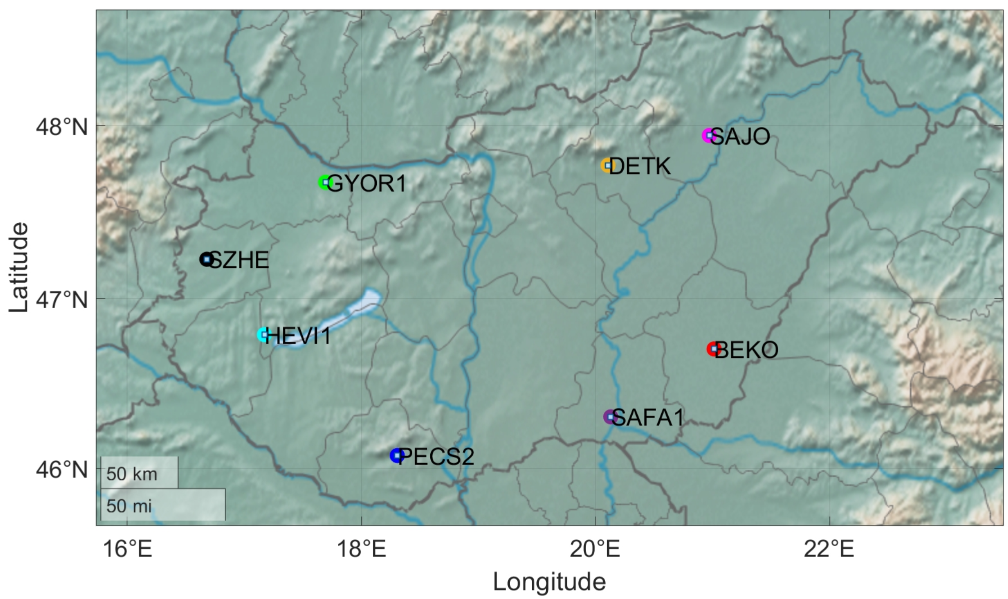

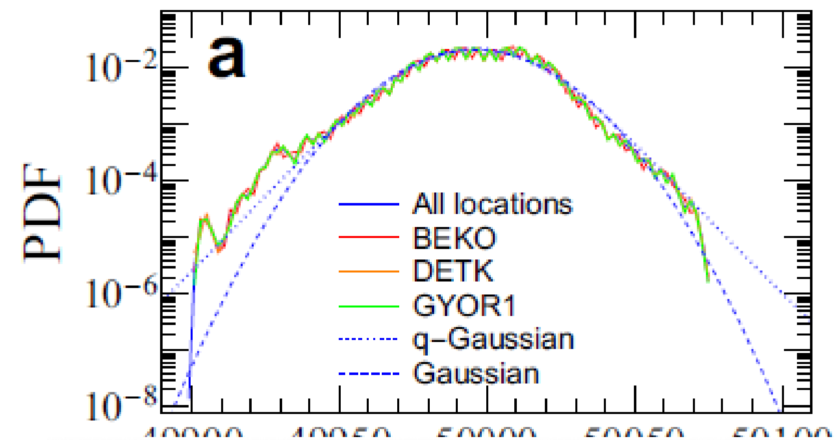

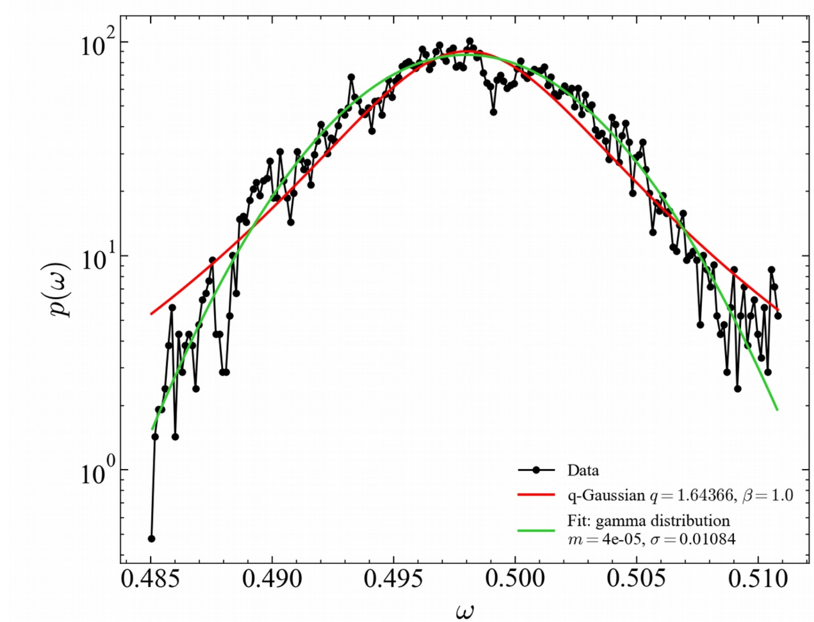

Frequency data in Hungary at 10/23 2022

Fits well with q-Gaussian *(q~1.1)* (*SEGAN*)

Kuramoto solution on a 387 node HV with

Real parararameters, in/out powers,

line admittances, inertias … etc

Comparison of frequency results with measurements of Hungarian HV power-grid

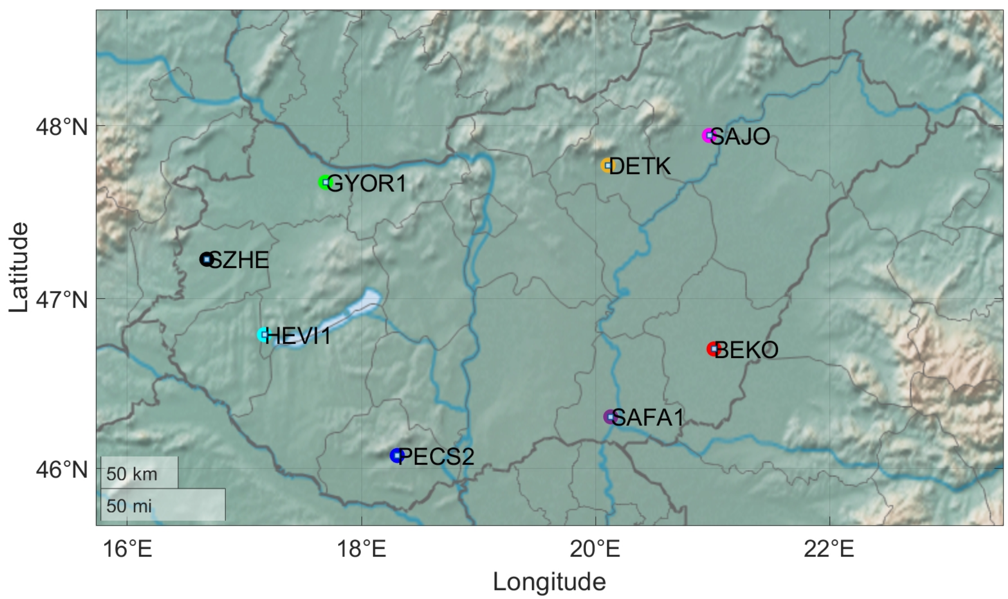

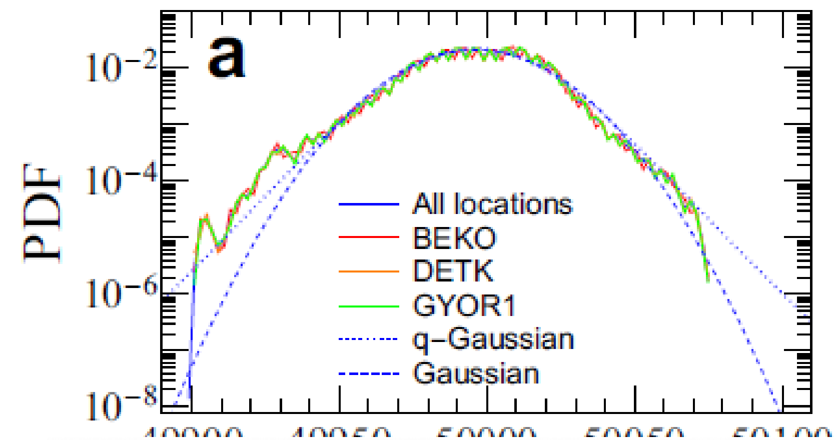

Frequency data in Hungary at 10/23 2022

Fits well with q-Gaussian *(q~1.1)* (*SEGAN*)

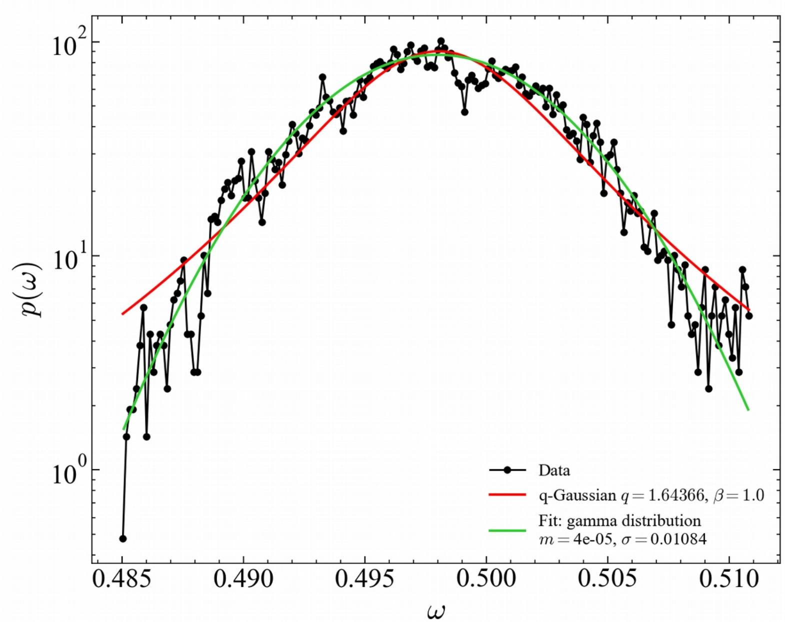

Kuramoto solution on a 387 node HV with

Real pararameters, in/out powers,

line admittances, inertias … etc

Fits well with q-Gaussian ***(q~1.6)***

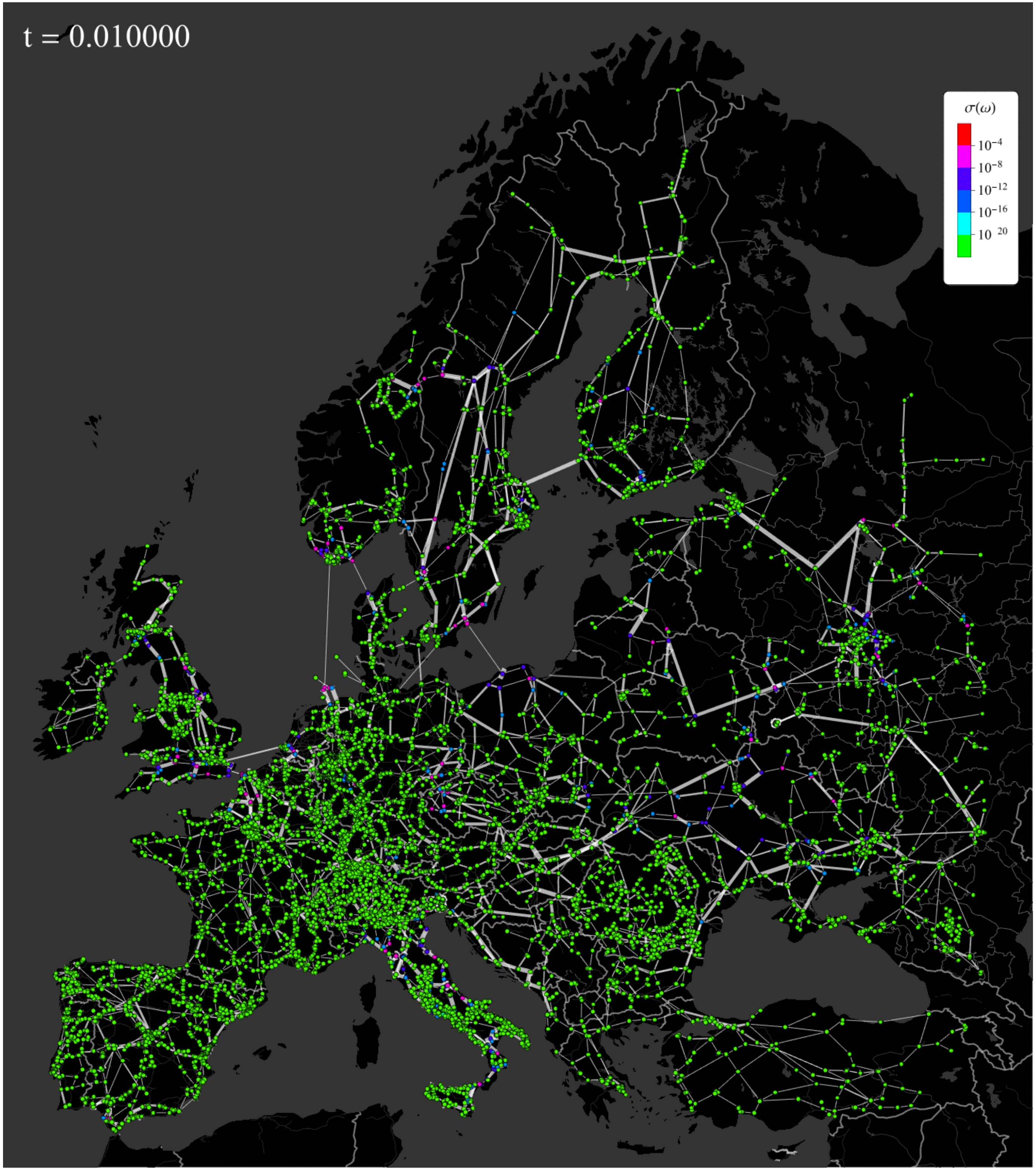

$$r_i(t) = \frac{1}{N_{i.\text{neigh}}} \left| \sum_j^{N_{i.\text{neigh}}} A_{ij} e^{i\theta_j(t)} \right|$$

Local frequency Synchronization during a blackout cascade, simulated by kuramotoGPU.

Chimera states: Deng and Ódor Chaos 2024

Stability improvement on power grids

Stability improvement on power grids

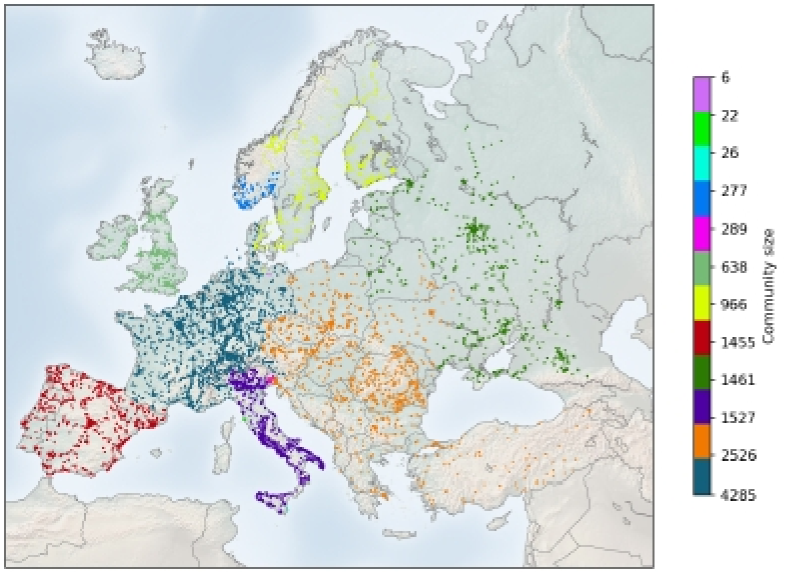

FIG. 9. All nodes of the European power-grid 2016 data separated into 12 communities, taking into account admittance, using a giant component of 13 478 nodes connected by 18 393 links, maintaining the modularity score close to the maximum $Q \approx 0.795$.

Stability improvement on power grids

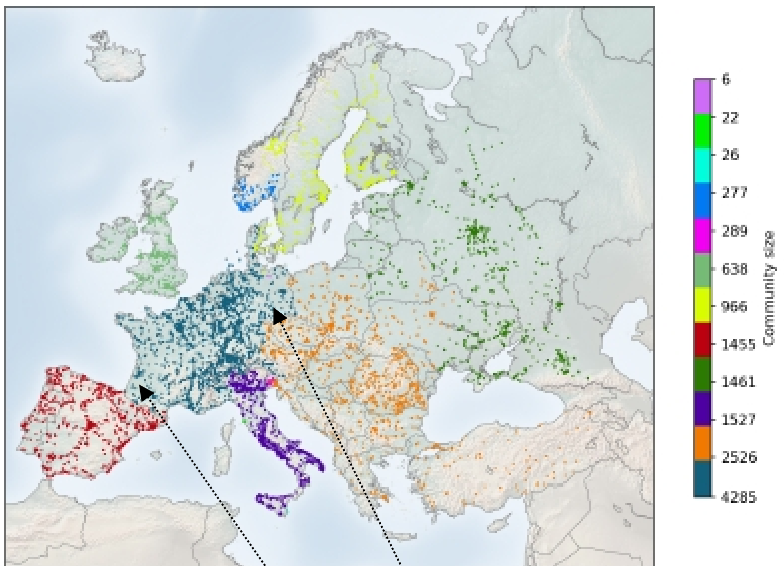

FIG. 9. All nodes of the European power-grid 2016 data separated into 12 communities, taking into account admittance, using a giant component of 13 478 nodes connected by 18 393 links, maintaining the modularity score close to the maximum $Q \approx 0.795$.

Improve by adding community bridges

Stability improvement on power grids

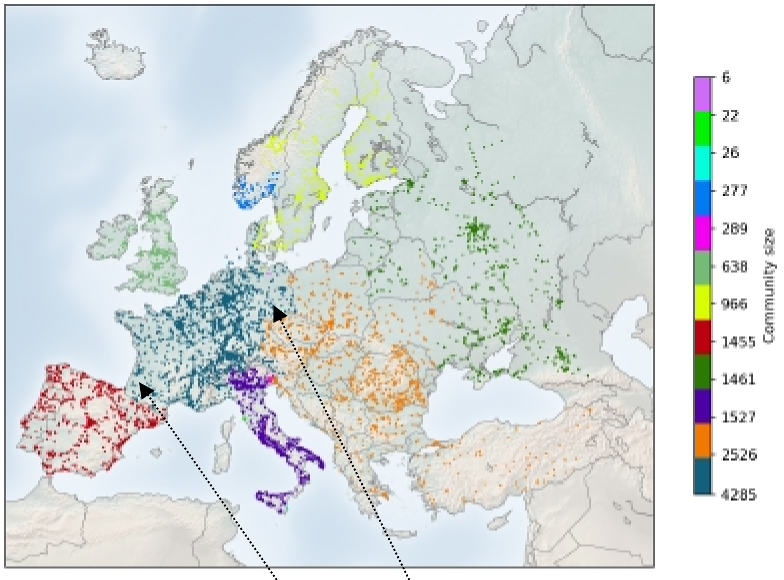

FIG. 9. All nodes of the European power-grid 2016 data separated into 12 communities, taking into account admittance, using a giant component of 13 478 nodes connected by 18 393 links, maintaining the modularity score close to the maximum $Q \approx 0.795$.

Improve by adding community bridges

Static

Stability improvement on power grids

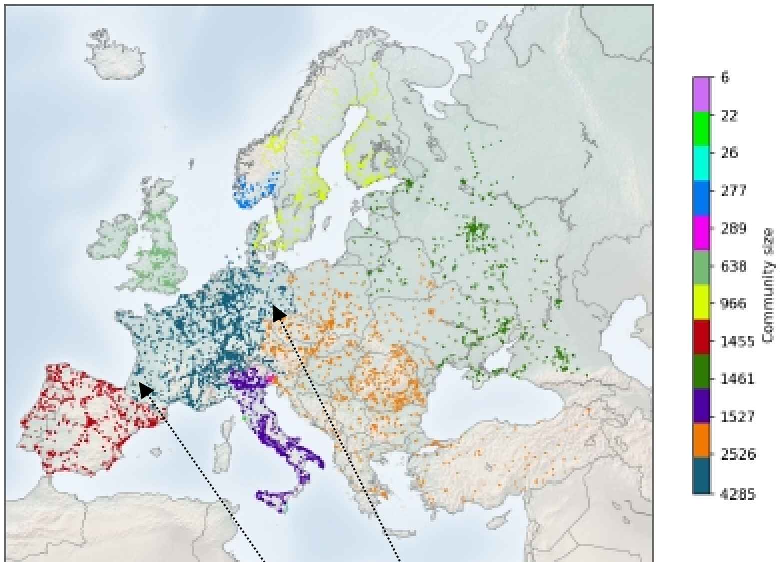

FIG. 9. All nodes of the European power-grid 2016 data separated into 12 communities, taking into account admittance, using a giant component of 13 478 nodes connected by 18 393 links, maintaining the modularity score close to the maximum $Q \approx 0.795$.

Improve by adding community bridges

Static

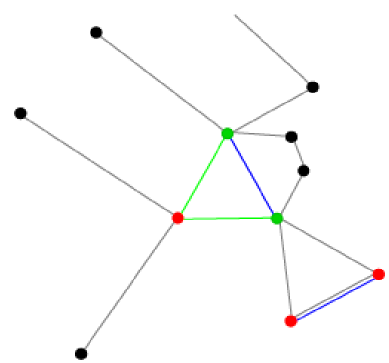

Or adding bypasses at weak local synchronization nodes

Stability improvement on power grids

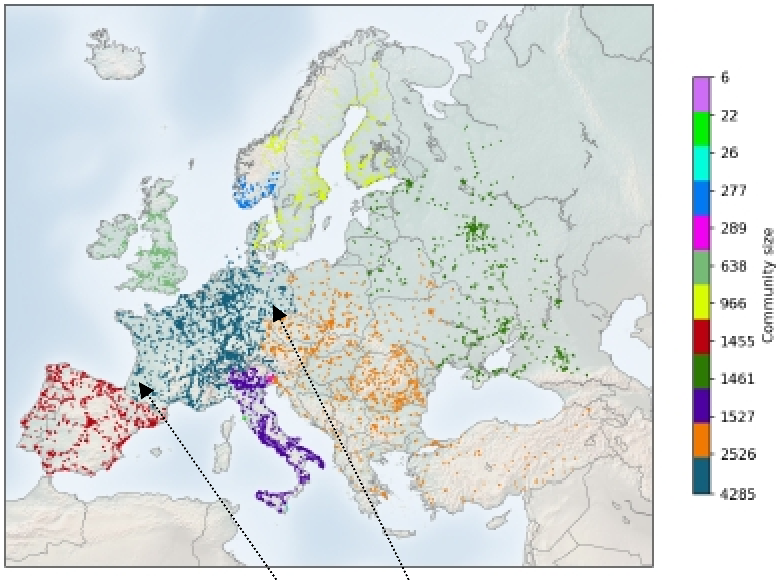

FIG. 9. All nodes of the European power-grid 2016 data separated into 12 communities, taking into account admittance, using a giant component of 13 478 nodes connected by 18 393 links, maintaining the modularity score close to the maximum $Q \approx 0.795$.

Improve by adding community bridges

Static

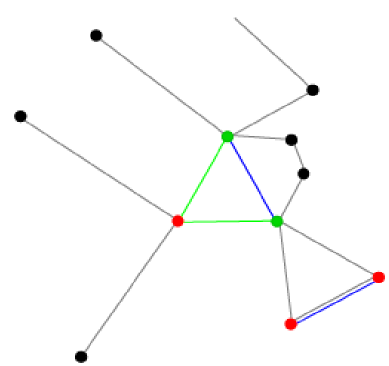

Or adding bypasses at weak local synchronization nodes

Dynamic

Stability improvement on power grids

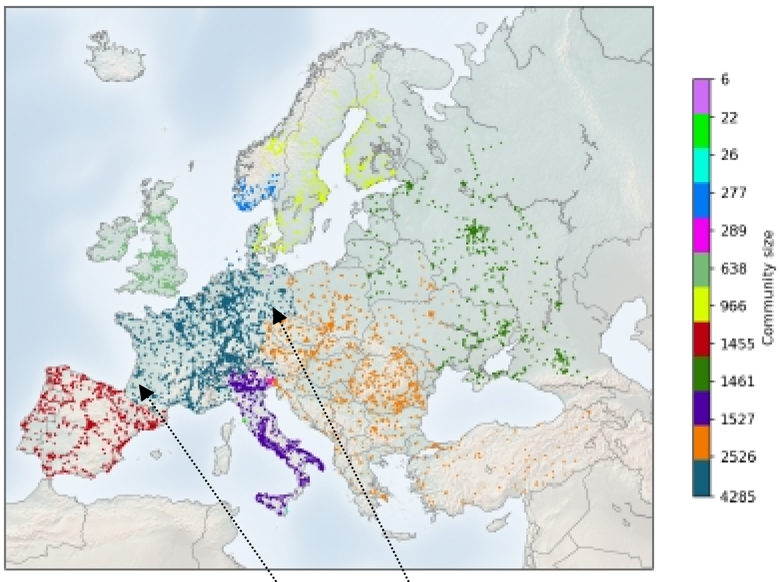

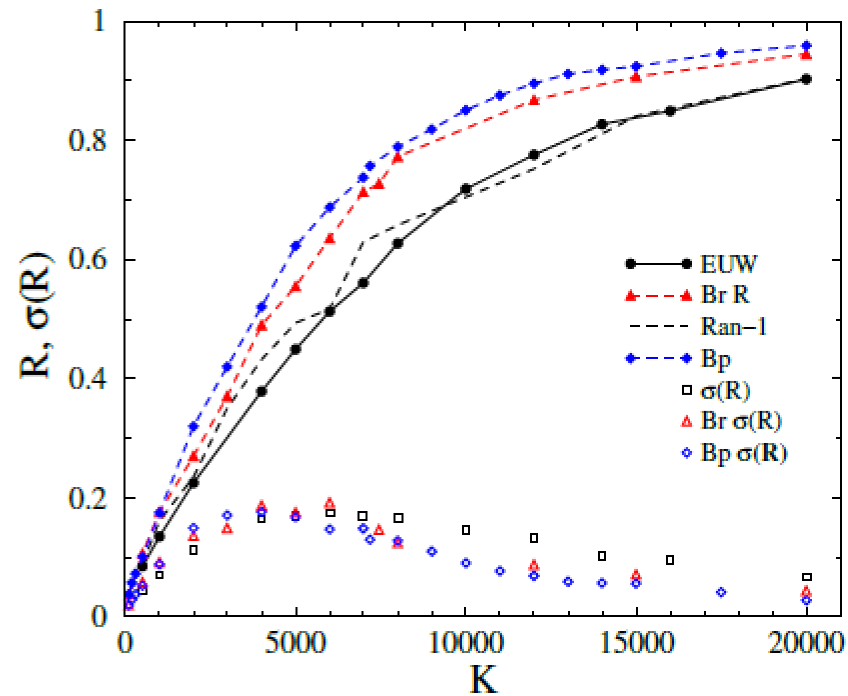

FIG. 9. All nodes of the European power-grid 2016 data separated into 12 communities, taking into account admittance, using a giant component of 13 478 nodes connected by 18 393 links, maintaining the modularity score close to the maximum $Q \approx 0.795$.

FIG. 5. Comparison of dynamical simulation results of R at the end of the thermalization for the original, randomly extended, bridged and bypassed networks, using $\alpha = 0.4$.

Improve by adding community bridges

Static

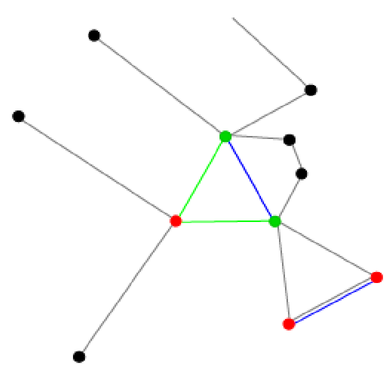

Or adding bypasses at weak local synchronization nodes

Dynamic

Braess Paradox and the SOC

Expansion plans in real power grids cause non-local overloads of the grid.

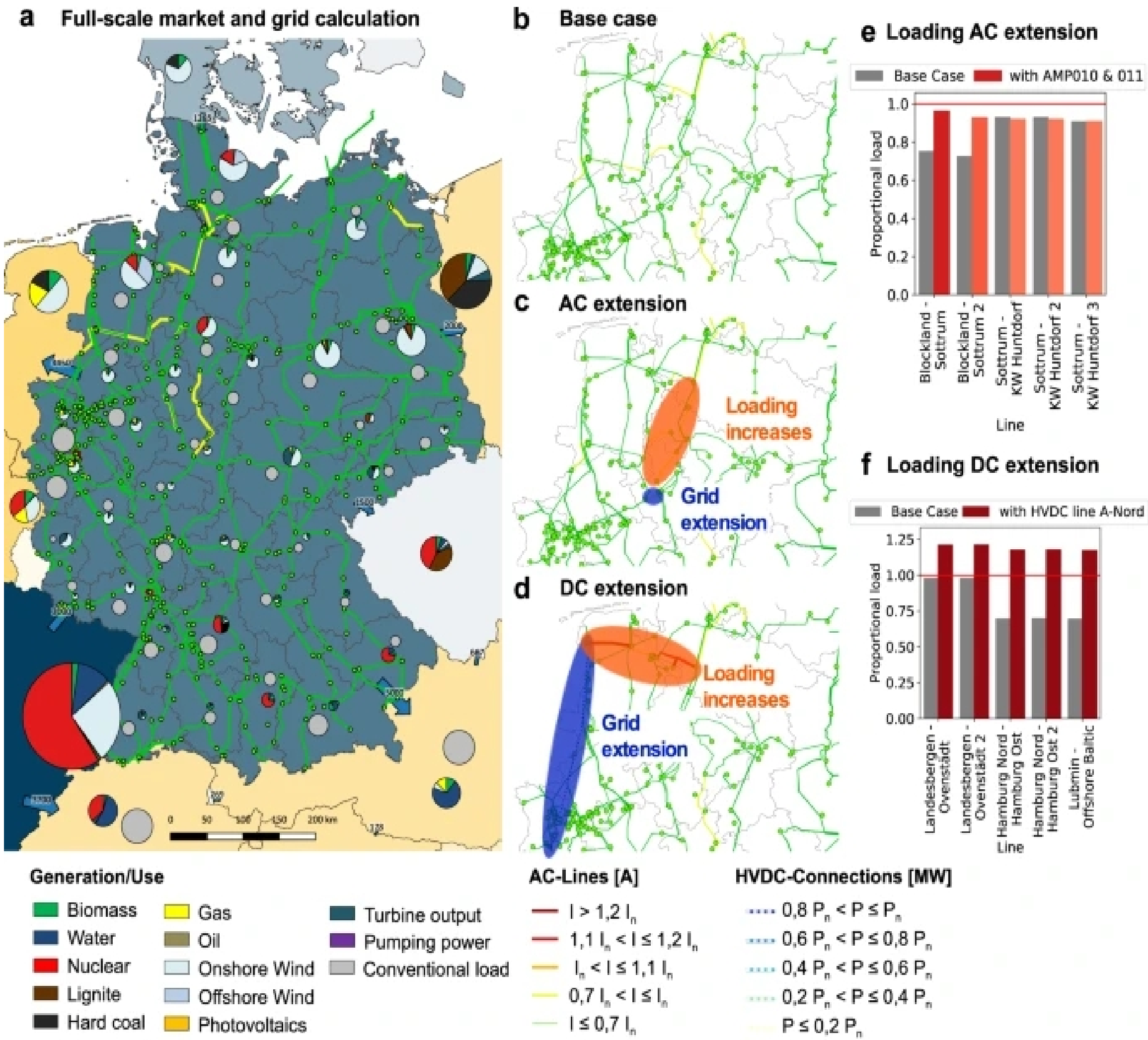

Schafer et al Nature Communications 13, 5396 (2022) 5396

Braess Paradox and the SOC

Expansion plans in real power grids cause non-local overloads of the grid.

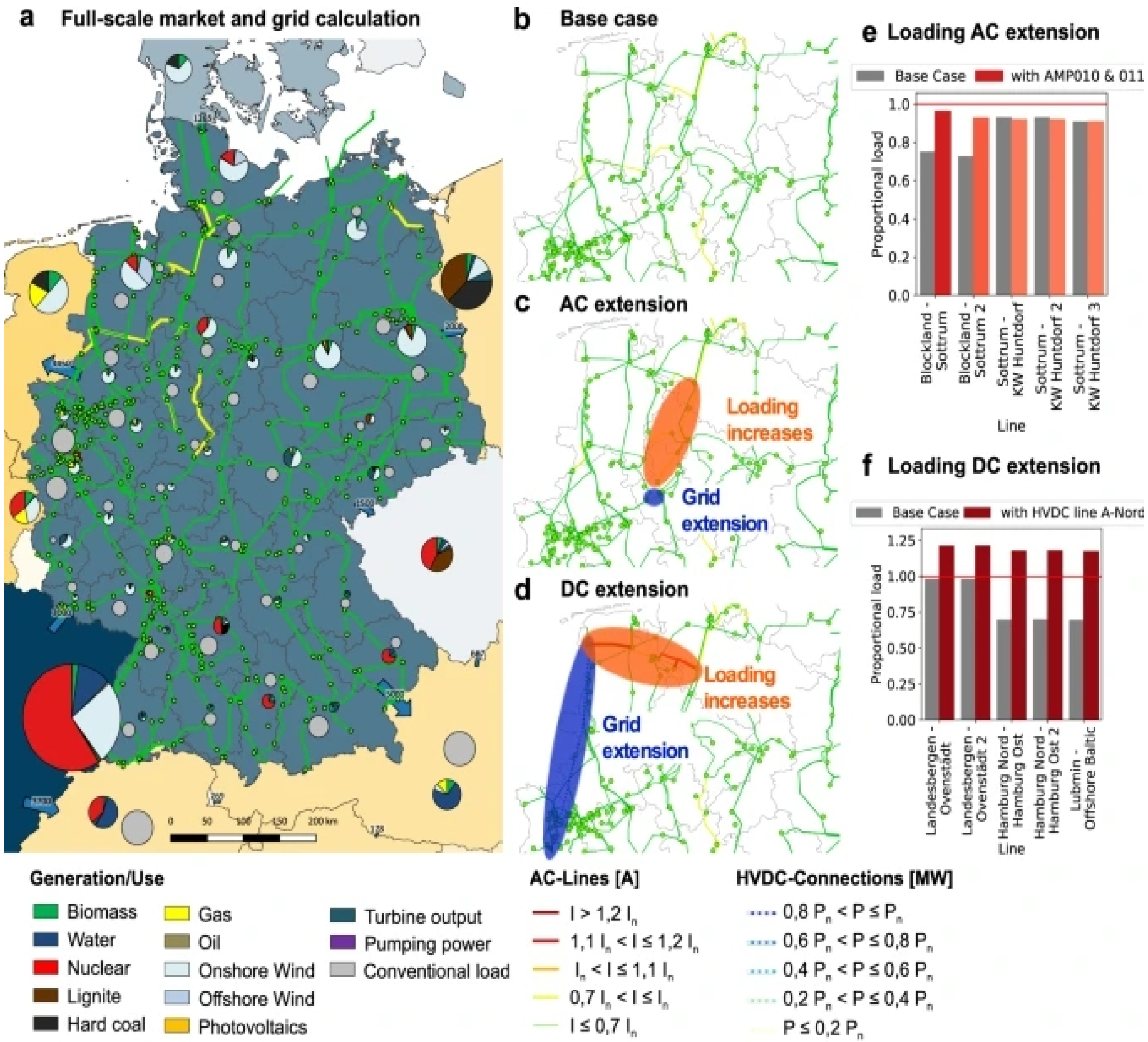

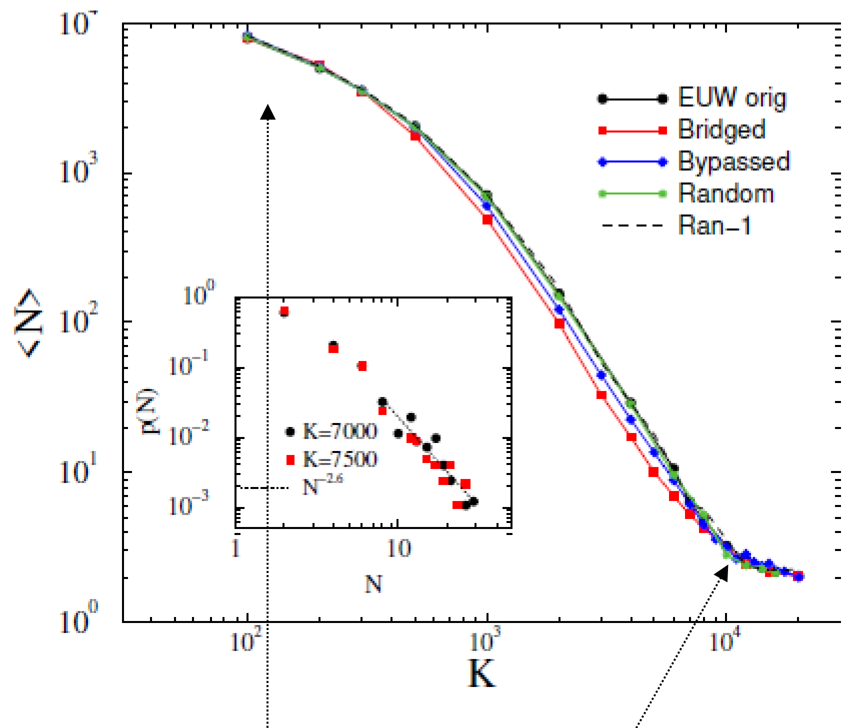

This happpens for low and high couplings, but not in the SOC region

Schafer et al Nature Communications 13, 5396 (2022) 5396

Conclusions

Conclusions

Efficient GPU synchronization simulations to describe blackouts on large AC networks

Conclusions

Efficient GPU synchronization simulations to describe blackouts on large AC networks

Non-local power-law cascade distributions, Dragon Kings, Island effects

Conclusions

Efficient GPU synchronization simulations to describe blackouts on large AC networks

Non-local power-law cascade distributions, Dragon Kings, Island effects

Enables us to analyze weak points of power-grids **FREQUENCY DATA** and

Conclusions

Efficient GPU synchronization simulations to describe blackouts on large AC networks

Non-local power-law cascade distributions, Dragon Kings, Island effects

Enables us to analyze weak points of power-grids **FREQUENCY DATA** and

Helps to design more stable grids

Conclusions

Efficient GPU synchronization simulations to describe blackouts on large AC networks

Non-local power-law cascade distributions, Dragon Kings, Island effects

Enables us to analyze weak points of power-grids **FREQUENCY DATA** and

Helps to design more stable grids

Empirical power-grid networks are

heterogeneous, still **universality** ***($N \to \infty$)***

Conclusions

Efficient GPU synchronization simulations to describe blackouts on large AC networks

Non-local power-law cascade distributions, Dragon Kings, Island effects

Enables us to analyze weak points of power-grids **FREQUENCY DATA** and

Helps to design more stable grids

Empirical power-grid networks are

heterogeneous, still **universality** $(N \to \infty)$

Reproducing frequency data well

in case of adequate parameters

Conclusions

Efficient GPU synchronization simulations to describe blackouts on large AC networks

Non-local power-law cascade distributions, Dragon Kings, Island effects

Enables us to analyze weak points of power-grids **FREQUENCY DATA** and

Helps to design more stable grids

Empirical power-grid networks are

heterogeneous, still **universality** ***($N \to \infty$)***

Reproducing frequency data well

in case of adequate parameters

Avoid Braess paradox by SOC

Conclusions

Efficient GPU synchronization simulations to describe blackouts on large AC networks

Non-local power-law cascade distributions, Dragon Kings, Island effects

Enables us to analyze weak points of power-grids **FREQUENCY DATA** and

Helps to design more stable grids

Empirical power-grid networks are

heterogeneous, still **universality** ***($N \to \infty$)***

Reproducing frequency data well

in case of adequate parameters

Avoid Braess paradox by SOC

Phys. Rev. Res. 6 (2024) 013194
SEGAN 2024 in press

Conclusions

Efficient GPU synchronization simulations to describe blackouts on large AC networks

Non-local power-law cascade distributions, Dragon Kings, Island effects

Enables us to analyze weak points of power-grids **FREQUENCY DATA** and

Helps to design more stable grids

Empirical power-grid networks are

heterogeneous, still **universality** ***($N \rightarrow \infty$)***

Reproducing frequency data well

in case of adequate parameters

Avoid Braess paradox by SOC

Phys. Rev. Res. 6 (2024) 013194
SEGAN 2024 in press

Recent, related publications:

Géza Ódor, Shengfeng Deng, ynchronization Transition of the Second-Order Kuramoto Model on Lattices
Entropy 25 (2023), 164

Géza Ódor, Shengfeng Deng, Balint Hartmann and Jeffrey Kelling
Synchronization dynamics on power grids in Europe and the United States,
Physical Review E 106 (2022) 034311.

Géza Ódor and Bálint Hartmann
Power-Law Distributions of Dynamic Cascade Failures in Power-Grid Models, **Entropy 22 (2020) 666**

Géza Ódor and Bálint Hartmann,
Heterogeneity effects in power grid network models
Phys. Rev. E 98 (2018) 022305

Conclusions

Efficient GPU synchronization simulations to describe blackouts on large AC networks

Non-local power-law cascade distributions, Dragon Kings, Island effects

Enables us to analyze weak points of power-grids **FREQUENCY DATA** and

Helps to design more stable grids

Empirical power-grid networks are

heterogeneous, still **universality** ***($N \to \infty$)***

Reproducing frequency data well

in case of adequate parameters

Avoid Braess paradox by SOC

Phys. Rev. Res. 6 (2024) 013194
SEGAN 2024 in press

Recent, related publications:

Géza Ódor, Shengfeng Deng, ynchronization Transition of the Second-Order Kuramoto Model on Lattices
Entropy 25 (2023), 164

Géza Ódor, Shengfeng Deng, Balint Hartmann and Jeffrey Kelling
Synchronization dynamics on power grids in Europe and the United States,
Physical Review E 106 (2022) 034311.

Géza Ódor and Bálint Hartmann
Power-Law Distributions of Dynamic Cascade Failures in Power-Grid Models, **Entropy 22 (2020) 666**

Géza Ódor and Bálint Hartmann,
Heterogeneity effects in power grid network models
Phys. Rev. E 98 (2018) 022305

Local synchronization study enables us to see non-local cascades

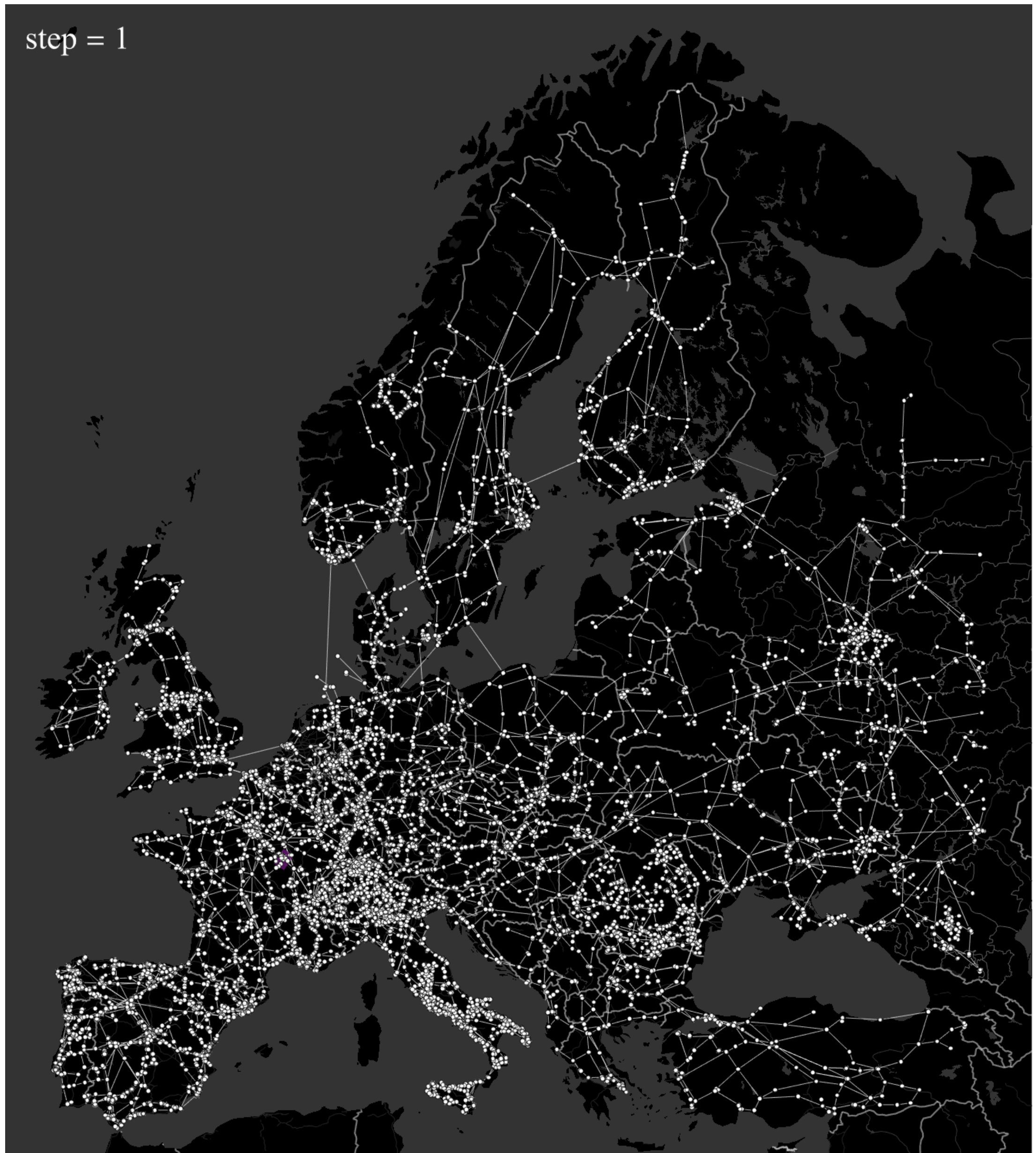

Local synchronization study enables us to see non-local cascades

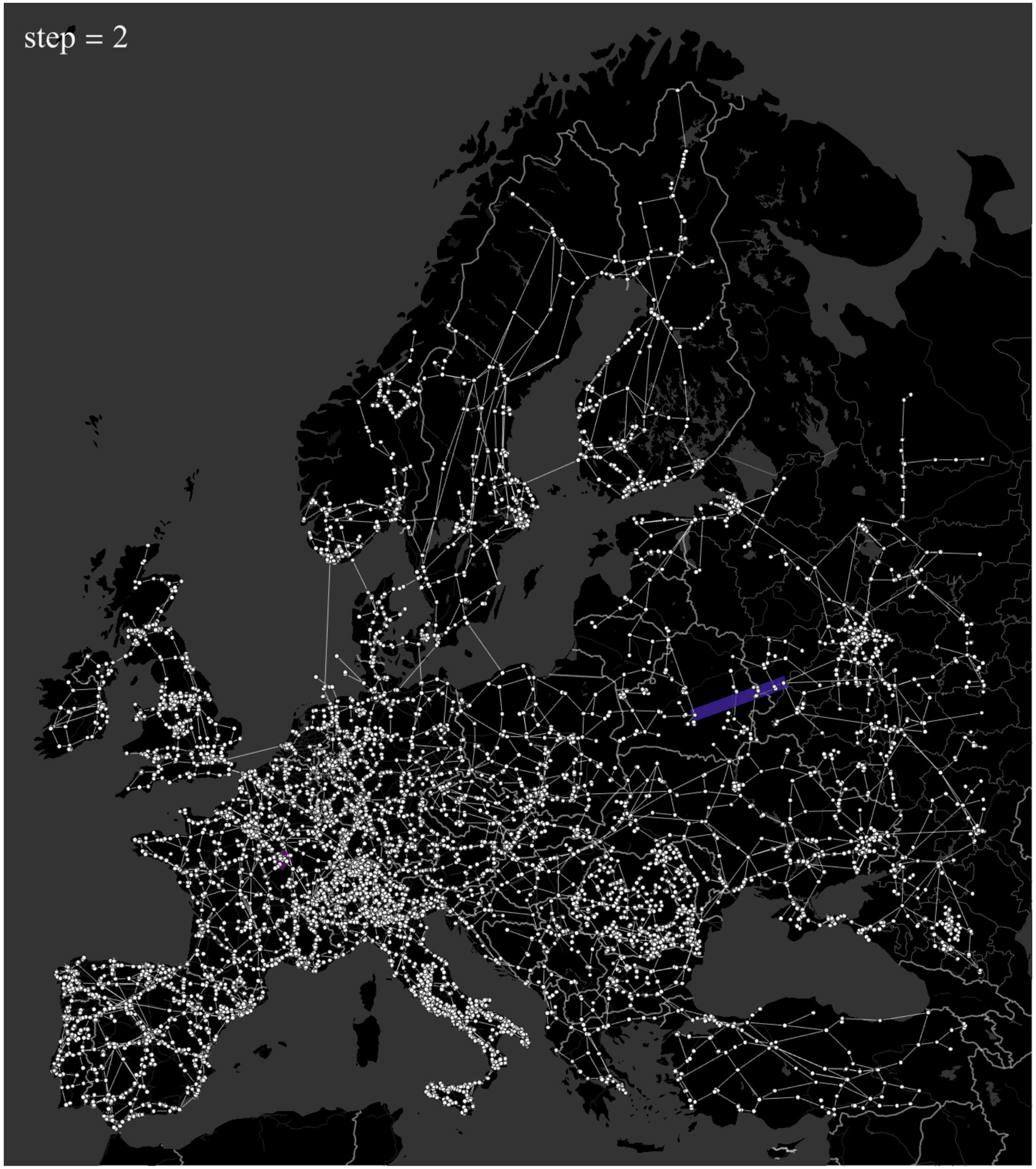

Local synchronization study enables us to see non-local cascades

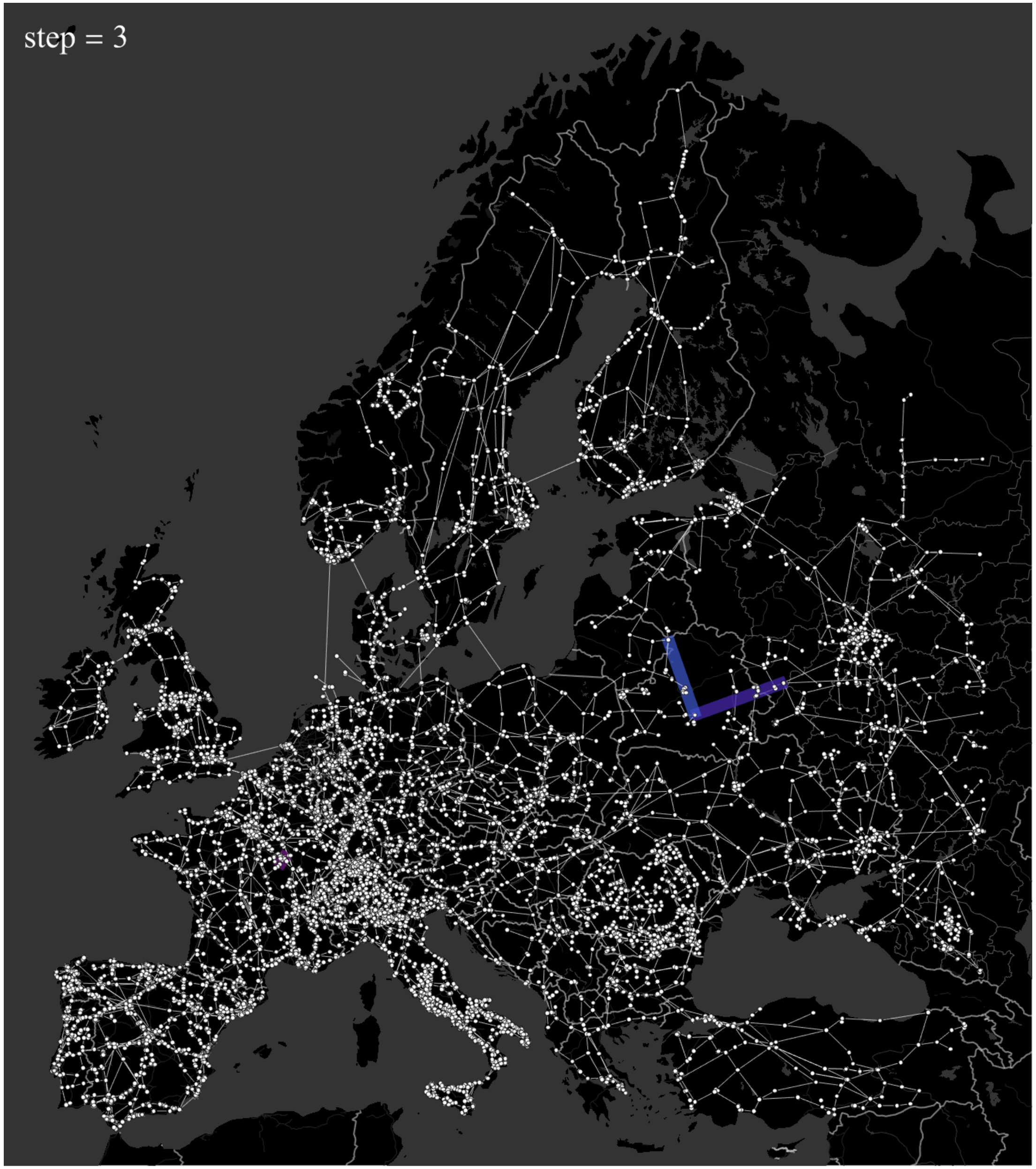

Local synchronization study enables us to see non-local cascades

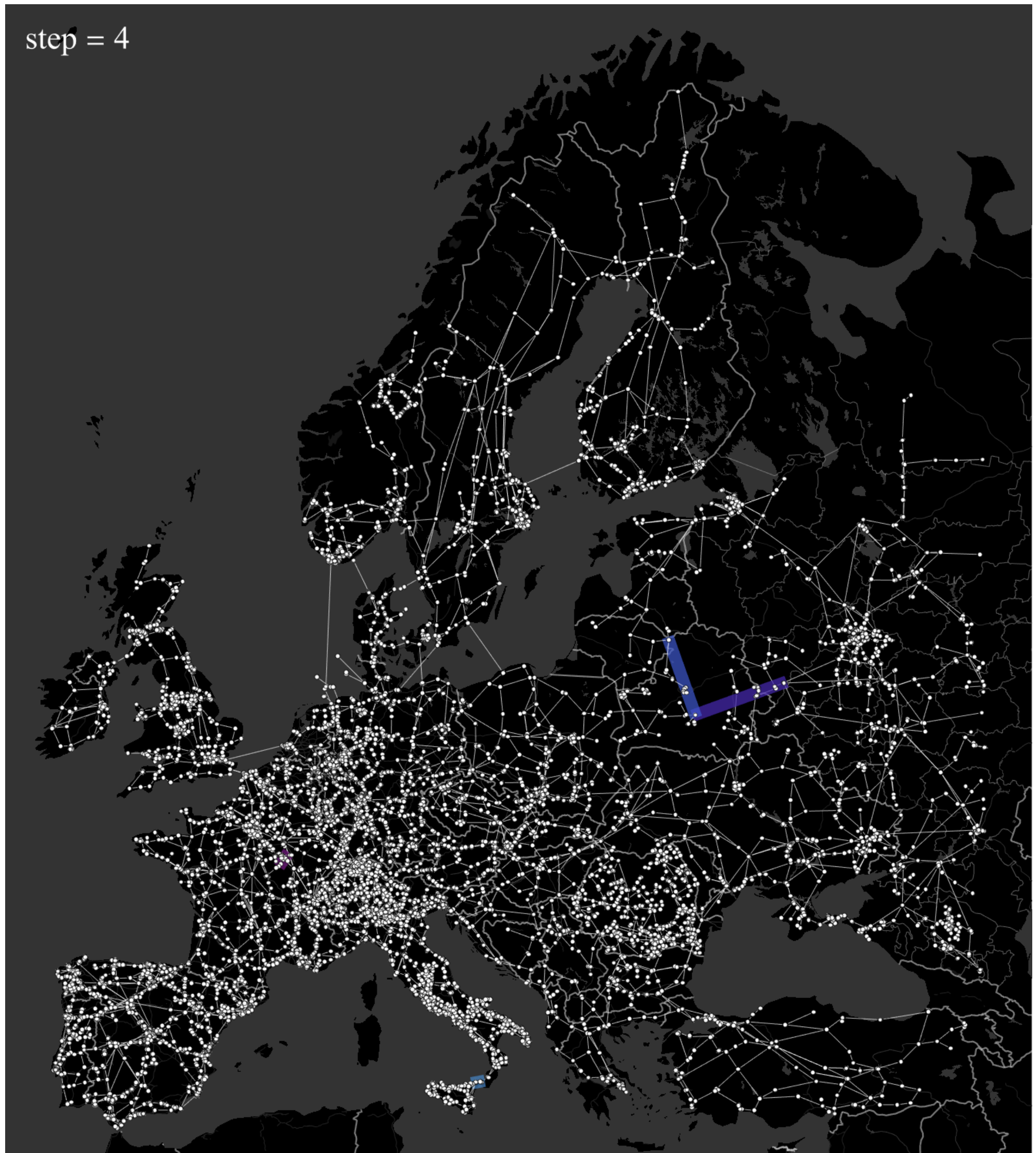

Local synchronization study enables us to see non-local cascades

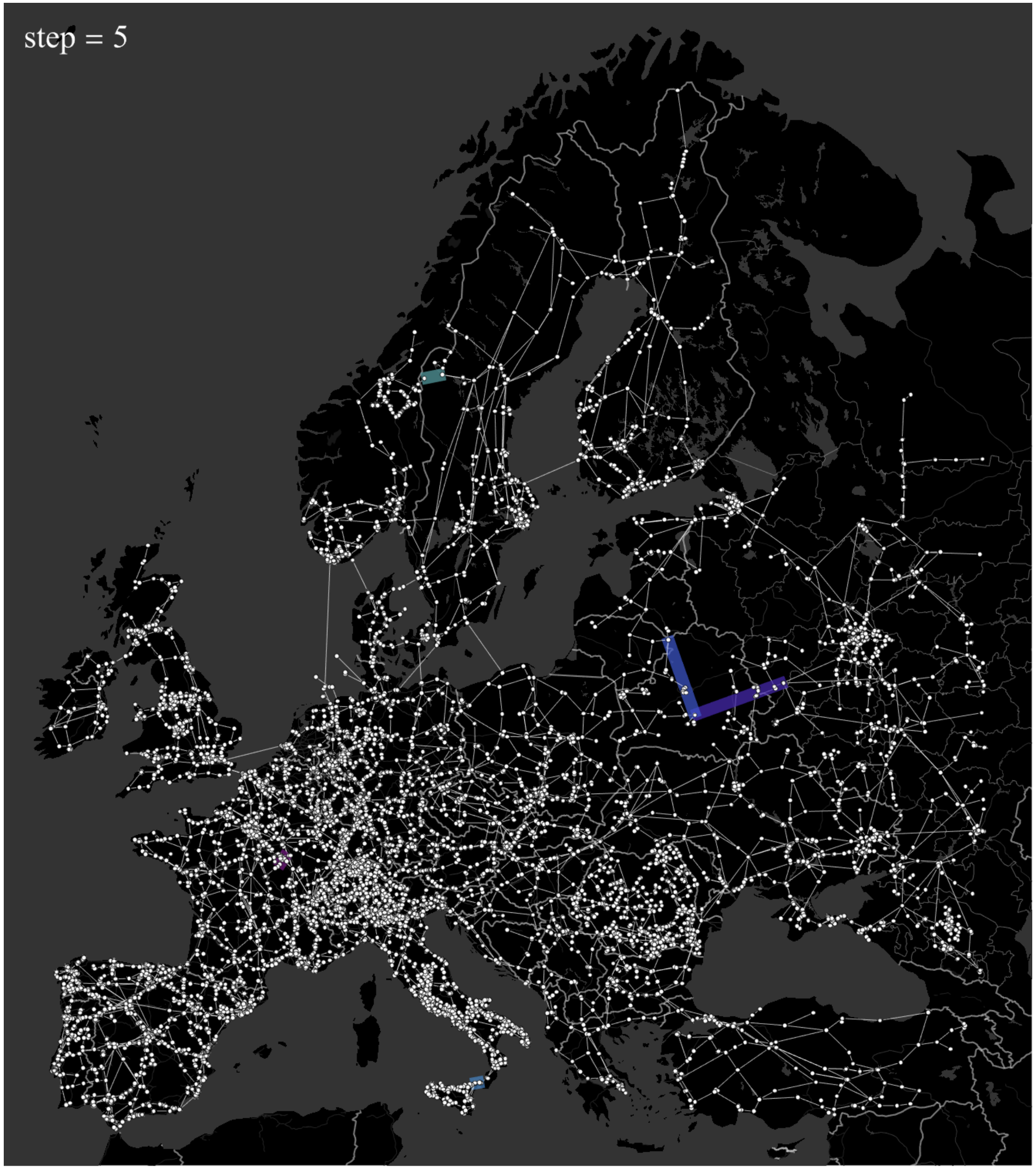

Local synchronization study enables us to see non-local cascades

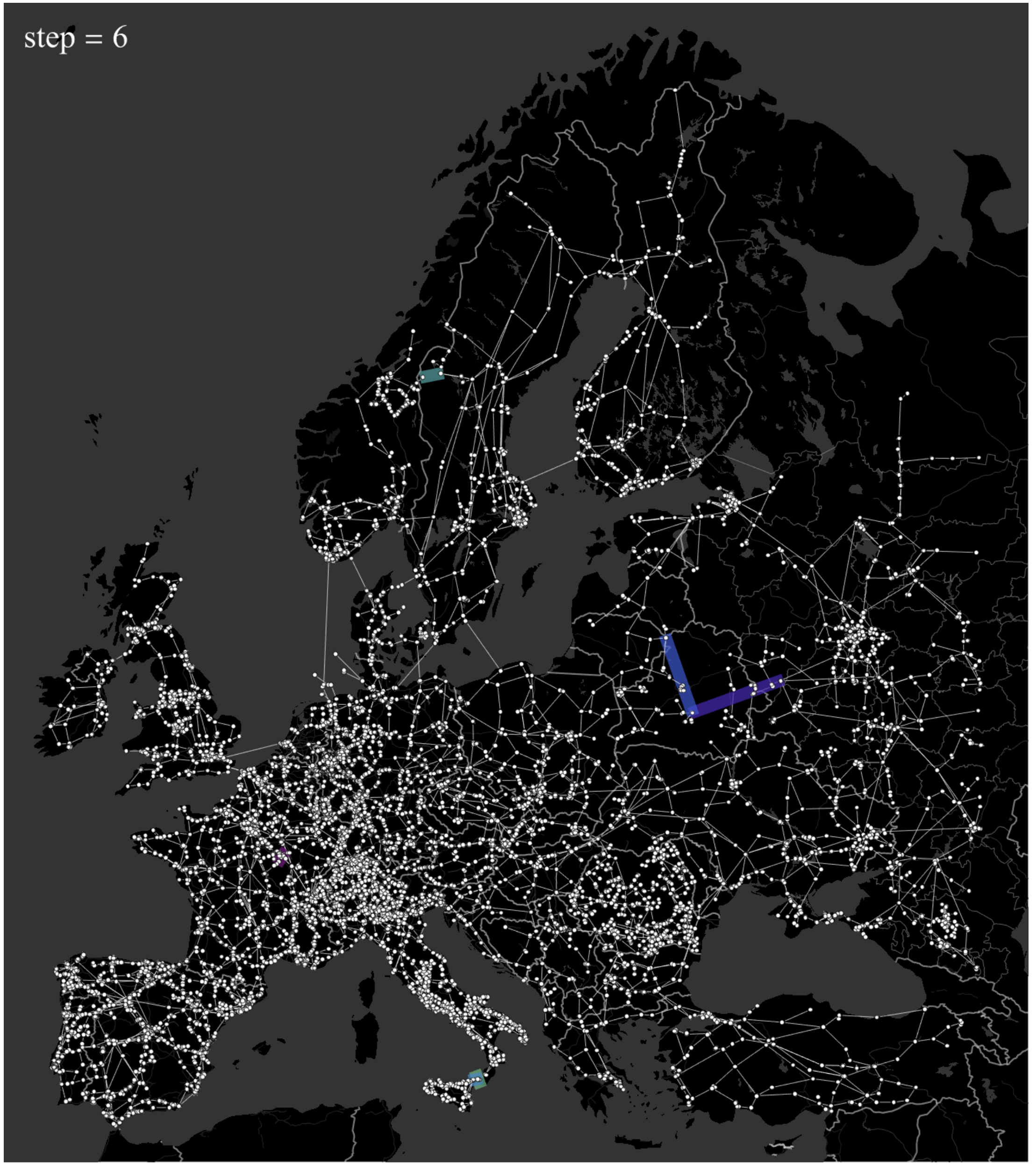

Local synchronization study enables us to see non-local cascades

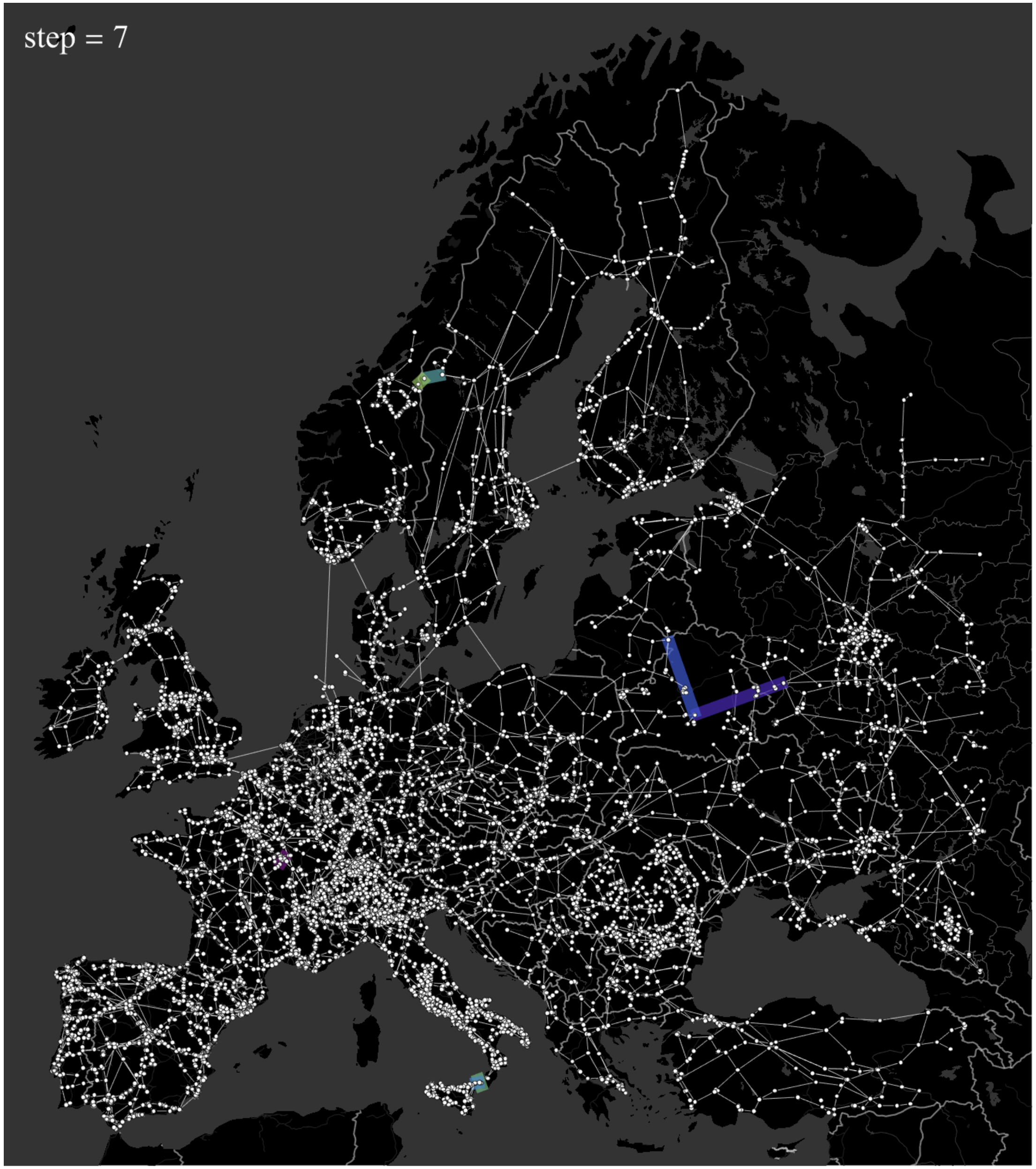

Local synchronization study enables us to see non-local cascades

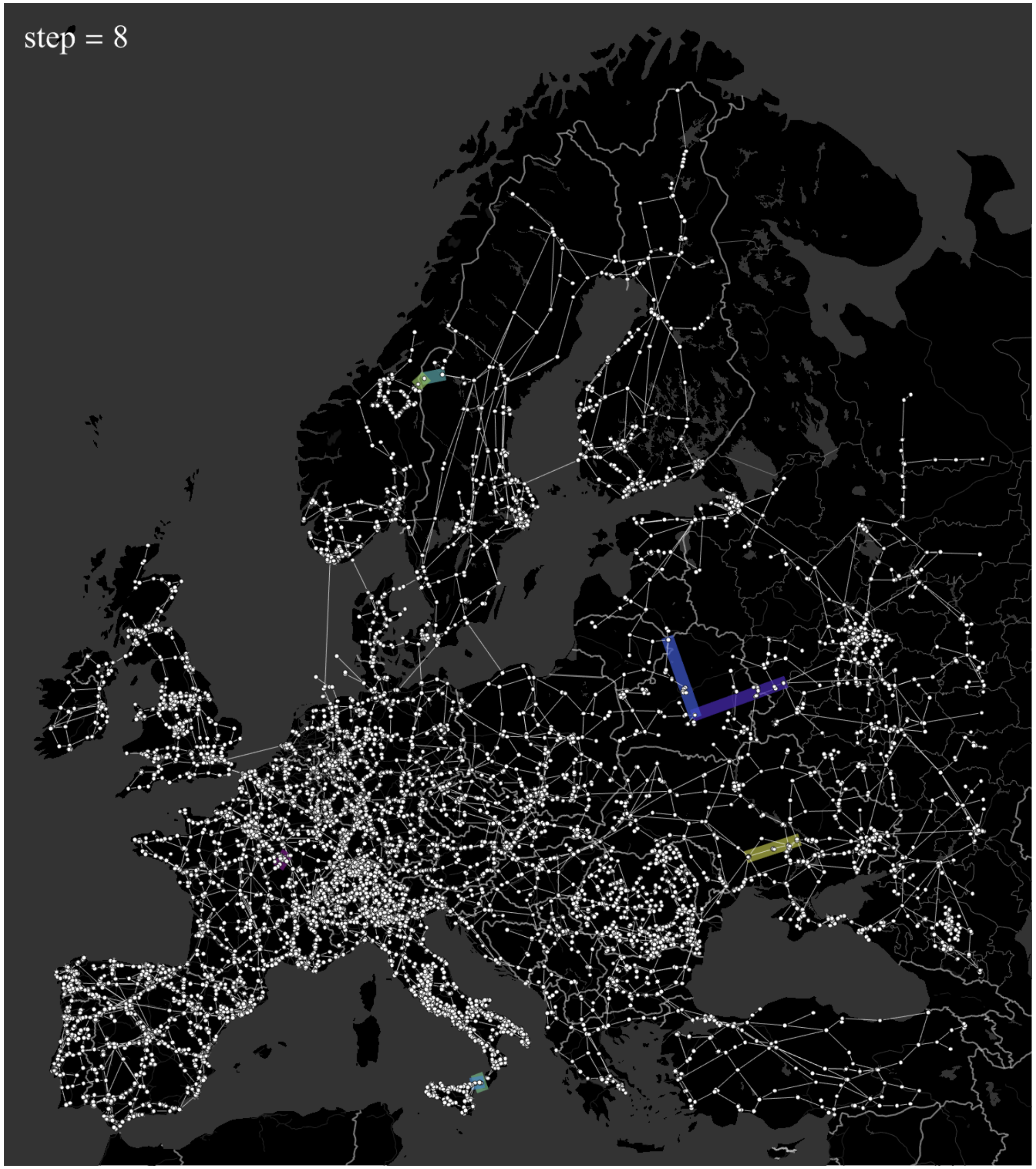

Local synchronization study enables us to see non-local cascades

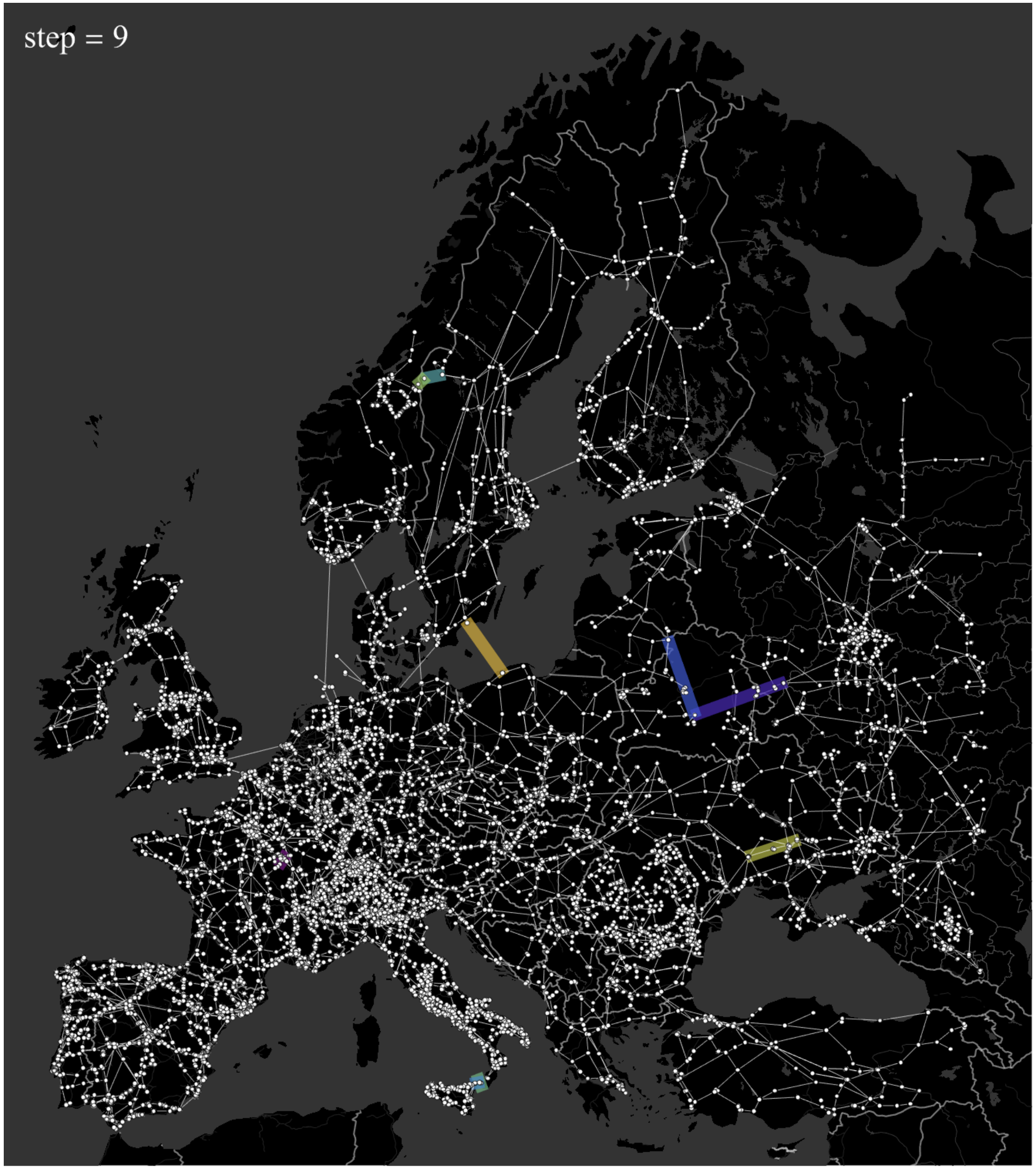

Local synchronization study enables us to see non-local cascades

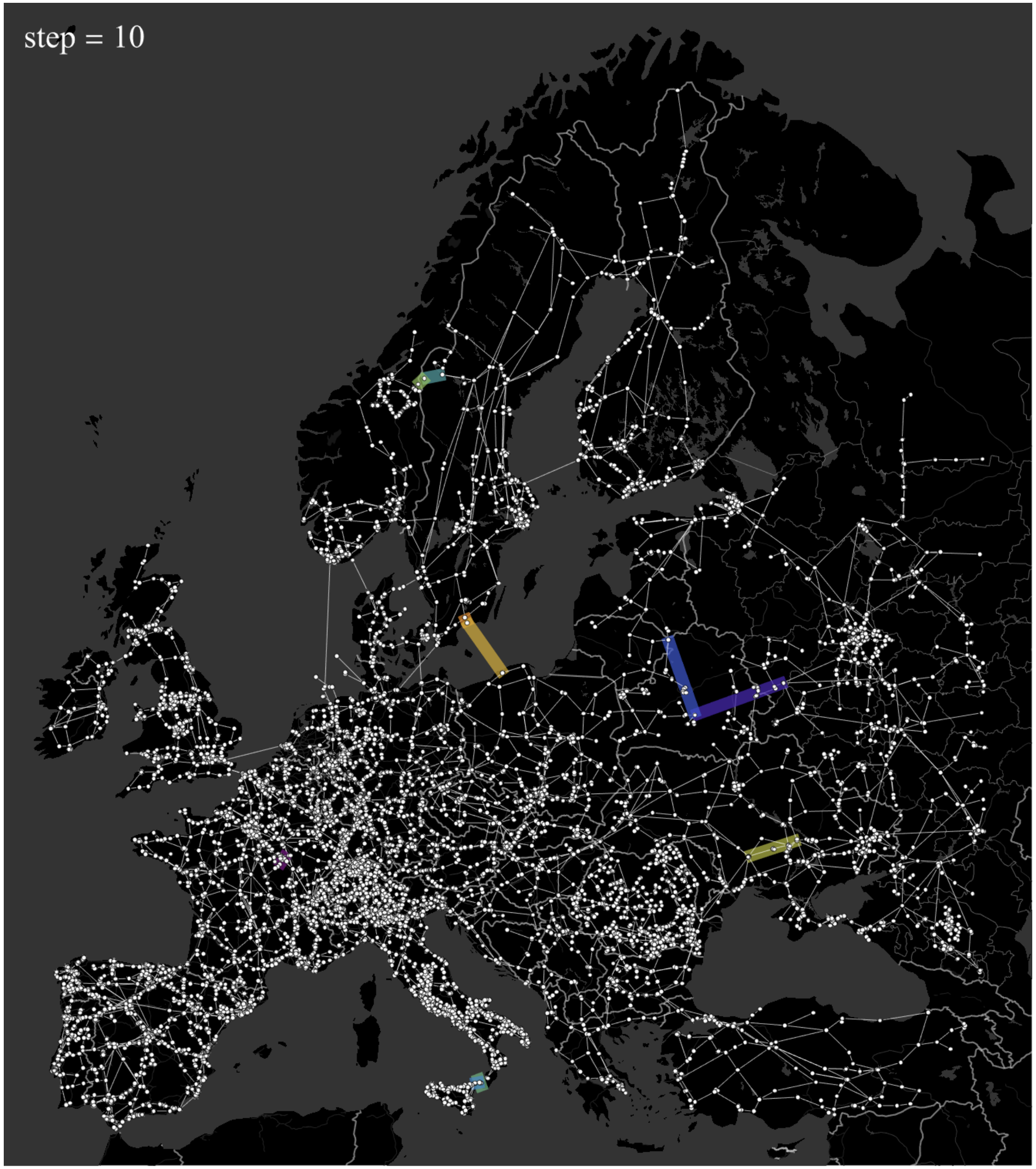

Local synchronization study enables us to see non-local cascades

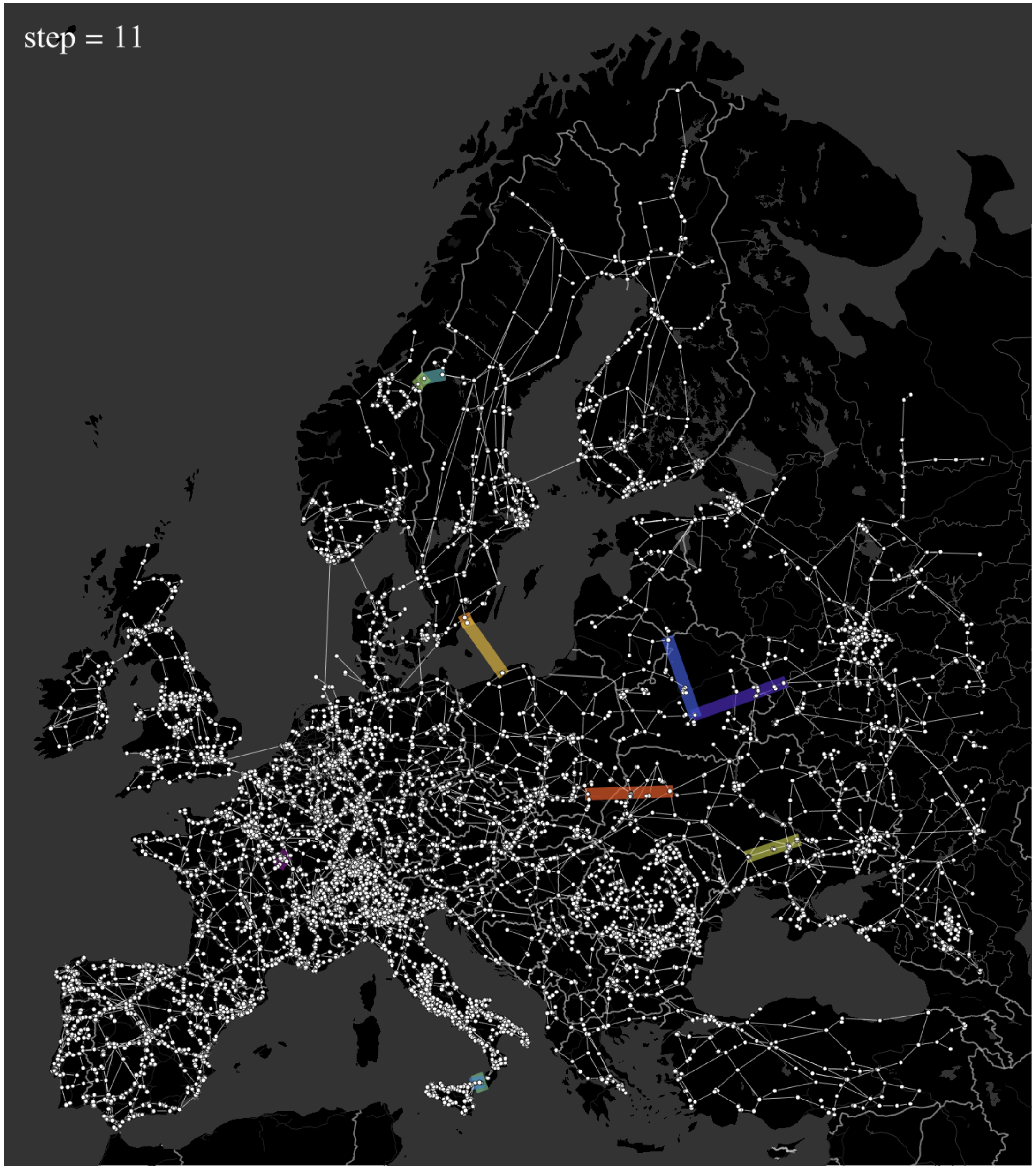

Outage durations with PL tails (digression)

Outage durations with PL tails (digression)

Electrical outages ≠ Blackout cascades, still they show PL duration

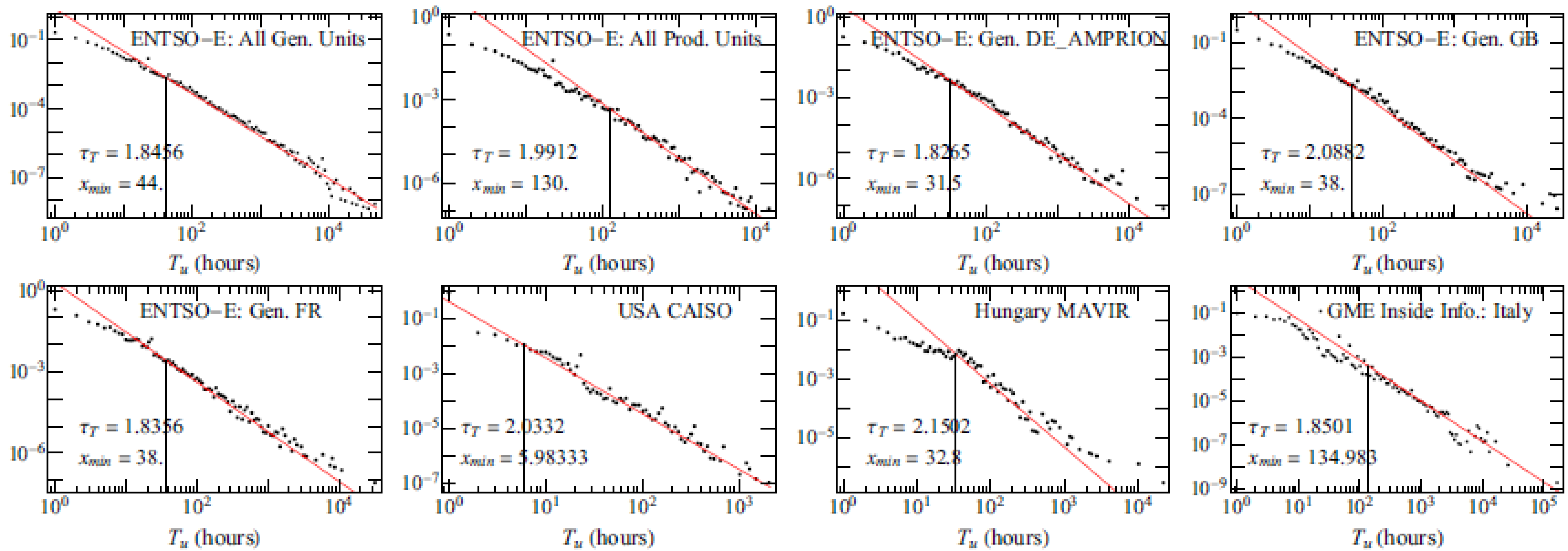

FIG. 2. Probability distributions (black dots) of generation outages measured in terms of the unavailable duration. For the ENTSO-E data, we show the generation outage data for the control areas "DE_AMPRION", "GB", and "FR", as well as the generation and production outage data from all control areas. The fitted power laws and their corresponding $x_{\min}$ values are marked by solid red lines and vertical black lines, respectively.

Outage durations with PL tails (digression)

Electrical outages ≠ Blackout cascades, still they show PL duration

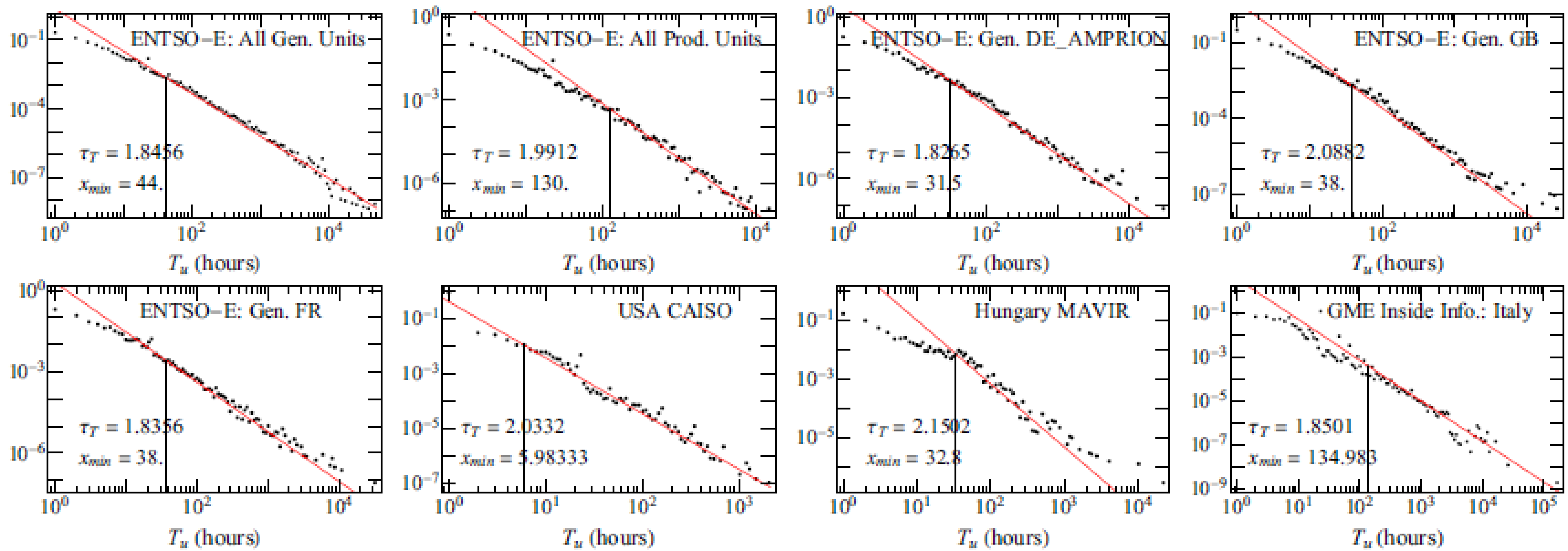

FIG. 2. Probability distributions (black dots) of generation outages measured in terms of the unavailable duration. For the ENTSO-E data, we show the generation outage data for the control areas “DE_AMPRION”, “GB”, and “FR”, as well as the generation and production outage data from all control areas. The fitted power laws and their corresponding x_{min} values are marked by solid red lines and vertical black lines, respectively.

Following power-spectral analysis we proposed SOC and HOT models to understand

See our recent paper : ***PRX Energy 2 (2023).033007***

Summary of community results

Community	Size (EU22)	$\langle k \rangle$ (EU22)	Size (EU16)	$\langle k \rangle$ (EU16)	Size (US16)	$\langle k \rangle$ (US16)
1	924	2.72	4285	2.83	3511	2.79
2	479	2.70	2526	2.66	2829	2.98
3	2016	2.84	1527	2.67	1640	2.72
4	698	3.06	1461	2.72	1484	2.69
5	595	2.94	1455	2.69	1396	2.93
6	1059	2.66	966	2.77	1165	2.58
7	1237	2.68	638	2.57	768	2.97
8	16	2.81	289	2.06	710	2.57
9	332	2.18	277	2.99	673	2.70
10	55	2.74	26	3.07	390	2.84
11	-	-	22	3.31	230	2.43
12	-	-	6	2.66	194	2.69

TABLE I. Community sizes and average degrees for different data-sets, for the resolution $\Gamma = 10^{-4}$. We refer to sizes here as number of nodes in the respecting community. These structures correspond to the maps plotted on Figs.9, 11, 12.

Louvain algorithm used with resolution

Parameter Γ

$$Q = \frac{1}{N\langle k \rangle} \sum_{ij} \left(A_{ij} - \Gamma \frac{k_i k_j}{N\langle k \rangle} \right) \delta(g_i, g_j),$$

Summary of community results

Community	Size (EU22)	$\langle k \rangle$ (EU22)	Size (EU16)	$\langle k \rangle$ (EU16)	Size (US16)	$\langle k \rangle$ (US16)
1	924	2.72	4285	2.83	3511	2.79
2	479	2.70	2526	2.66	2829	2.98
3	2016	2.84	1527	2.67	1640	2.72
4	698	3.06	1461	2.72	1484	2.69
5	595	2.94	1455	2.69	1396	2.93
6	1059	2.66	966	2.77	1165	2.58
7	1237	2.68	638	2.57	768	2.97
8	16	2.81	289	2.06	710	2.57
9	332	2.18	277	2.99	673	2.70
10	55	2.74	26	3.07	390	2.84
11	-	-	22	3.31	230	2.43
12	-	-	6	2.66	194	2.69

TABLE I. Community sizes and average degrees for different data-sets, for the resolution $\Gamma = 10^{-4}$. We refer to sizes here as number of nodes in the respecting community. These structures correspond to the maps plotted on Figs.9, 11, 12.

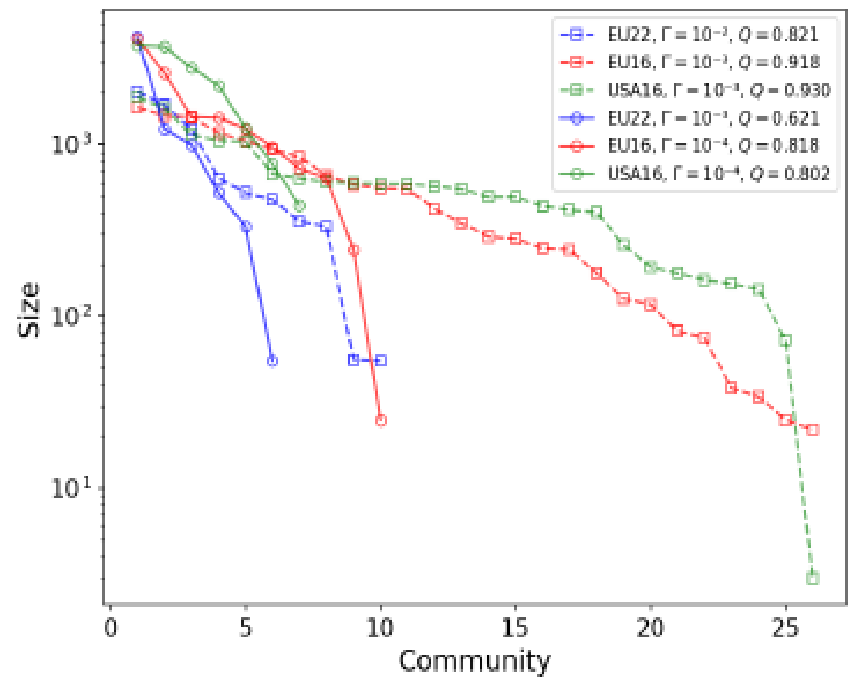

FIG. 8. Community size distributions at different Γ resolution parameters for different networks shown in the legend.

Louvain algorithm used with resolution

Parameter Γ

$$Q = \frac{1}{N\langle k \rangle} \sum_{ij} \left(A_{ij} - \Gamma \frac{k_i k_j}{N \langle k \rangle} \right) \delta(g_i, g_j),$$

Admittances (interaction weights), calculated from cable lengths and specific resistances

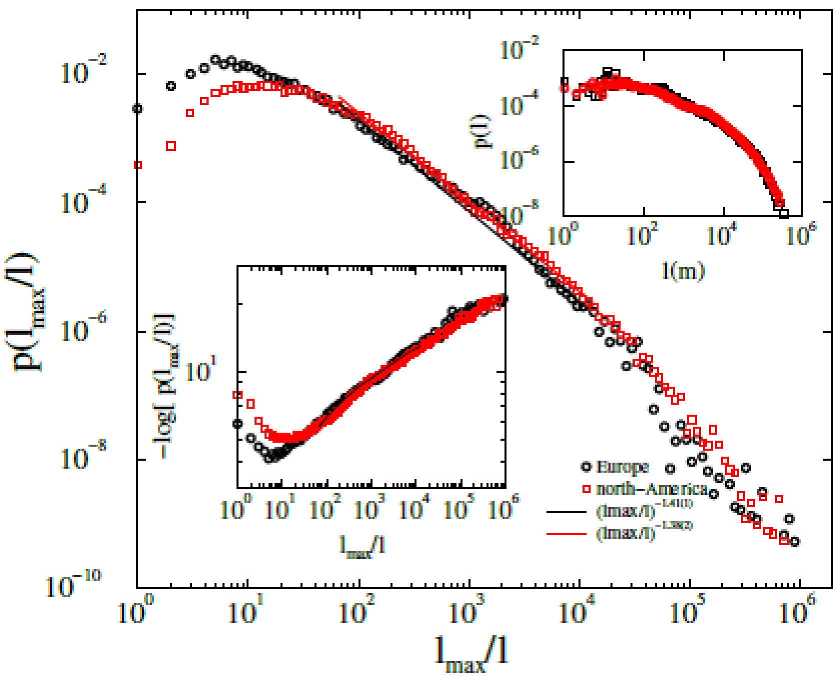

FIG. 14. Probability distributions of the inverse of cable lengths of the European and North-American SciGRID networks. Left inset: the same data plotted on the $-\ln(p)$ scale to compare with the stretched exponential assumption, that would correspond to a straight line tail, Right inset: probability distributions of the line lengths in meters.

Admittances (interaction weights), calculated from cable lengths and specific resistances

$$R_{ij} = \left(\frac{U_c}{U_{ij}}\right)^2 \cdot L_{ij} \cdot R_{c_k}$$

$$X_{ij} = \left(\frac{U_c}{U_{ij}}\right)^2 \cdot L_{ij} \cdot X_{c_k}$$

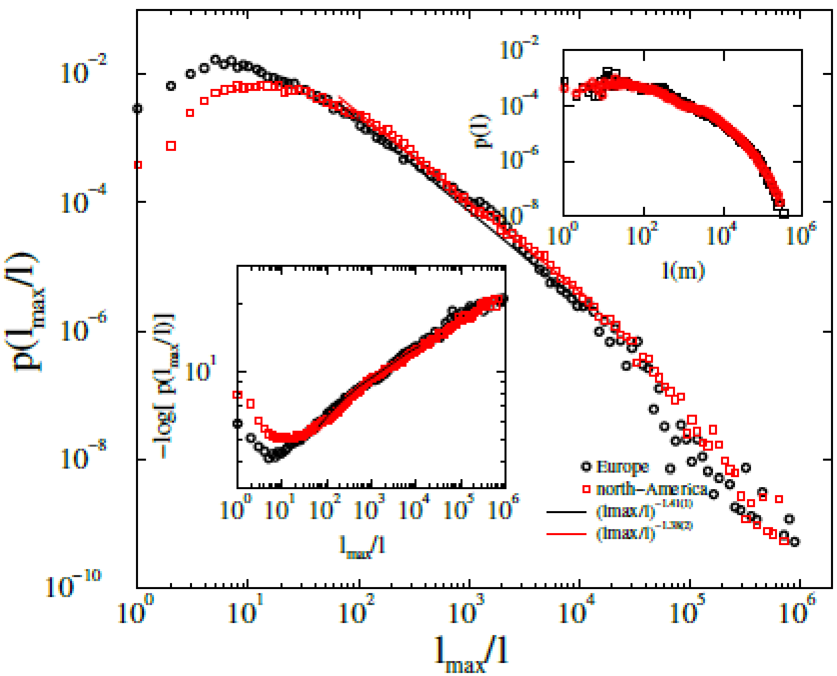

FIG. 14. Probability distributions of the inverse of cable lengths of the European and North-American SciGRID networks. Left inset: the same data plotted on the $-\ln(p)$ scale to compare with the stretched exponential assumption, that would correspond to a straight line tail, Right inset: probability distributions of the line lengths in meters.

Admittances (interaction weights), calculated from cable lengths and specific resistances

$$R_{ij} = \left(\frac{U_c}{U_{ij}}\right)^2 \cdot L_{ij} \cdot R_{c_k} \qquad P_{ij} = P_{c_k},$$

$$X_{ij} = \left(\frac{U_c}{U_{ij}}\right)^2 \cdot L_{ij} \cdot X_{c_k}$$

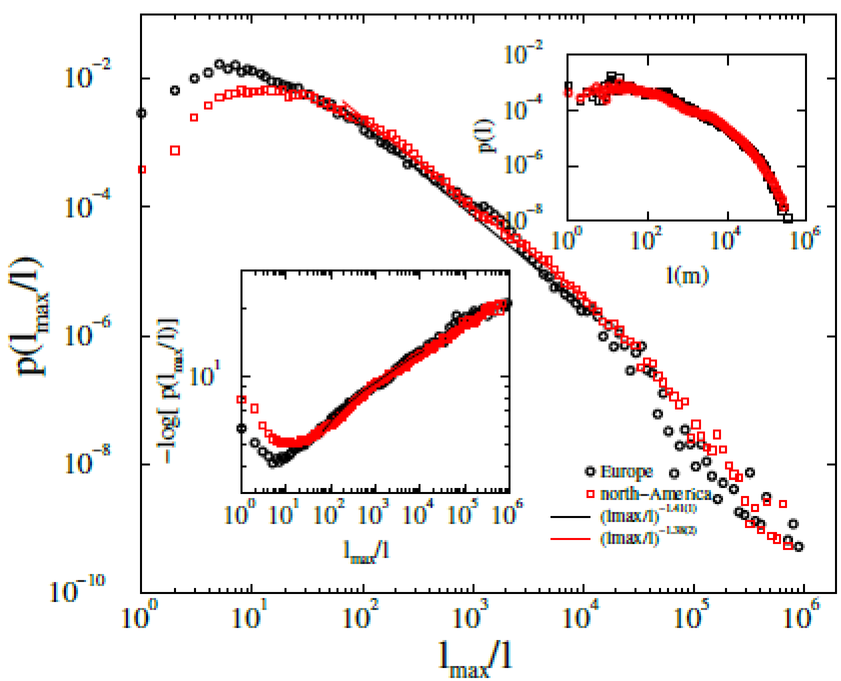

FIG. 14. Probability distributions of the inverse of cable lengths of the European and North-American SciGRID networks. Left inset: the same data plotted on the $-\ln(p)$ scale to compare with the stretched exponential assumption, that would correspond to a straight line tail, Right inset: probability distributions of the line lengths in meters.

Admittances (interaction weights), calculated from cable lengths and specific resistances

$$R_{ij} = \left(\frac{U_c}{U_{ij}}\right)^2 \cdot L_{ij} \cdot R_{c_k} \qquad P_{ij} = P_{c_k},$$

$$X_{ij} = \left(\frac{U_c}{U_{ij}}\right)^2 \cdot L_{ij} \cdot X_{c_k} \qquad W_{ij} = \frac{P_{ij}}{X_{ij}} \Big/ \left\langle \frac{P}{X} \right\rangle$$

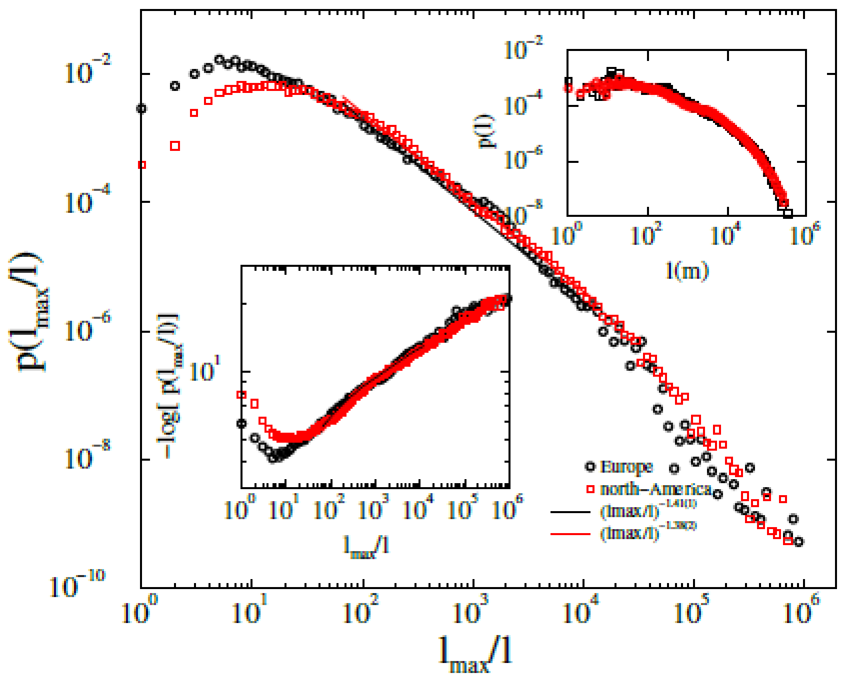

FIG. 14. Probability distributions of the inverse of cable lengths of the European and North-American SciGRID networks. Left inset: the same data plotted on the $-\ln(p)$ scale to compare with the stretched exponential assumption, that would correspond to a straight line tail, Right inset: probability distributions of the line lengths in meters.

TABLE II. Characteristic values of relevant physical quantities in the modeled European power grids.

Voltage [kV]	R_c [Ω/km]	X_c [Ω/km]	C_c [nF/km]	P_c [MW]
120	0.0293	0.1964	9.4	170
220	0.0293	0.2085	9.0	360
380/400	0.0286	0.3384	10.8	1300

Admittances (interaction weights), calculated from cable lengths and specific resistances

$$R_{ij} = \left(\frac{U_c}{U_{ij}}\right)^2 \cdot L_{ij} \cdot R_{c_k} \qquad P_{ij} = P_{c_k},$$

$$X_{ij} = \left(\frac{U_c}{U_{ij}}\right)^2 \cdot L_{ij} \cdot X_{c_k} \qquad W_{ij} = \frac{P_{ij}}{X_{ij}} \Big/ \left\langle \frac{P}{X} \right\rangle$$

TABLE II. Characteristic values of relevant physical quantities in the modeled European power grids.

Voltage [kV]	R_c [Ω/km]	X_c [Ω/km]	C_c [nF/km]	P_c [MW]
120	0.0293	0.1964	9.4	170
220	0.0293	0.2085	9.0	360
380/400	0.0286	0.3384	10.8	1300

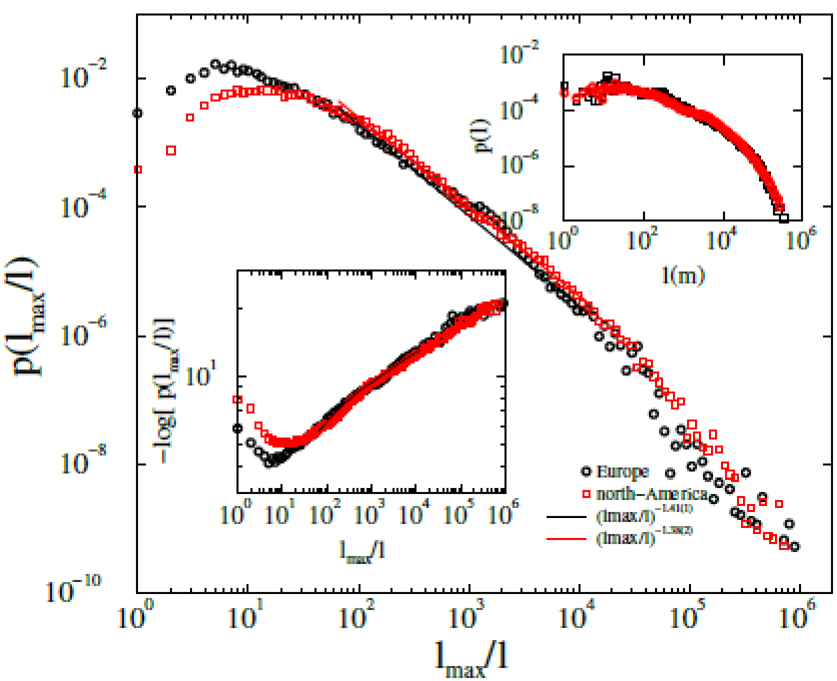

FIG. 14. Probability distributions of the inverse of cable lengths of the European and North-American SciGRID networks. Left inset: the same data plotted on the $-\ln(p)$ scale to compare with the stretched exponential assumption, that would correspond to a straight line tail, Right inset: probability distributions of the line lengths in meters.

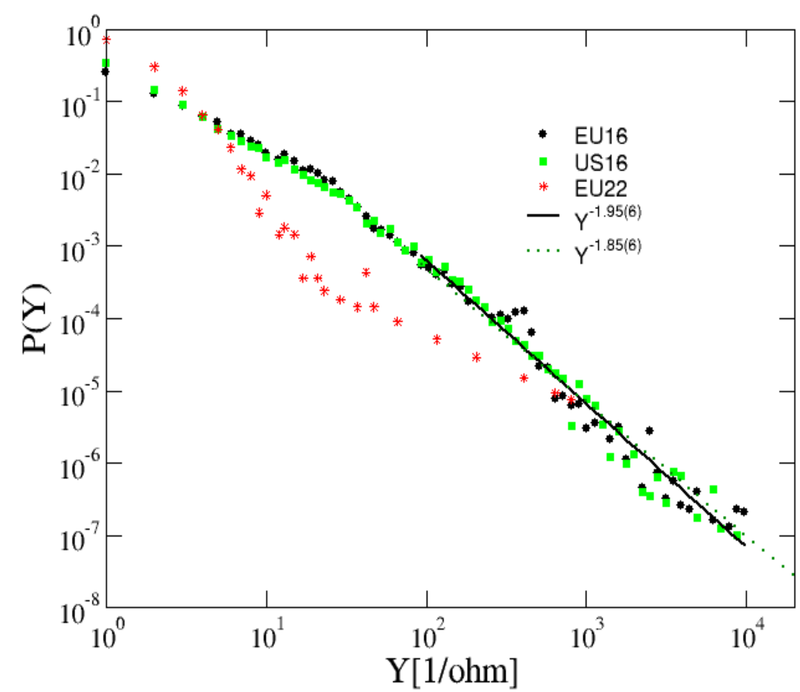

Admittances (interaction weights), calculated from cable lengths and specific resistances

$$R_{ij} = \left(\frac{U_c}{U_{ij}}\right)^2 \cdot L_{ij} \cdot R_{c_k} \qquad P_{ij} = P_{c_k},$$

$$X_{ij} = \left(\frac{U_c}{U_{ij}}\right)^2 \cdot L_{ij} \cdot X_{c_k} \qquad W_{ij} = \frac{P_{ij}}{X_{ij}} \Big/ \left\langle \frac{P}{X} \right\rangle$$

TABLE II. Characteristic values of relevant physical quantities in the modeled European power grids.

Voltage [kV]	R_c [Ω/km]	X_c [Ω/km]	C_c [nF/km]	P_c [MW]
120	0.0293	0.1964	9.4	170
220	0.0293	0.2085	9.0	360
380/400	0.0286	0.3384	10.8	1300

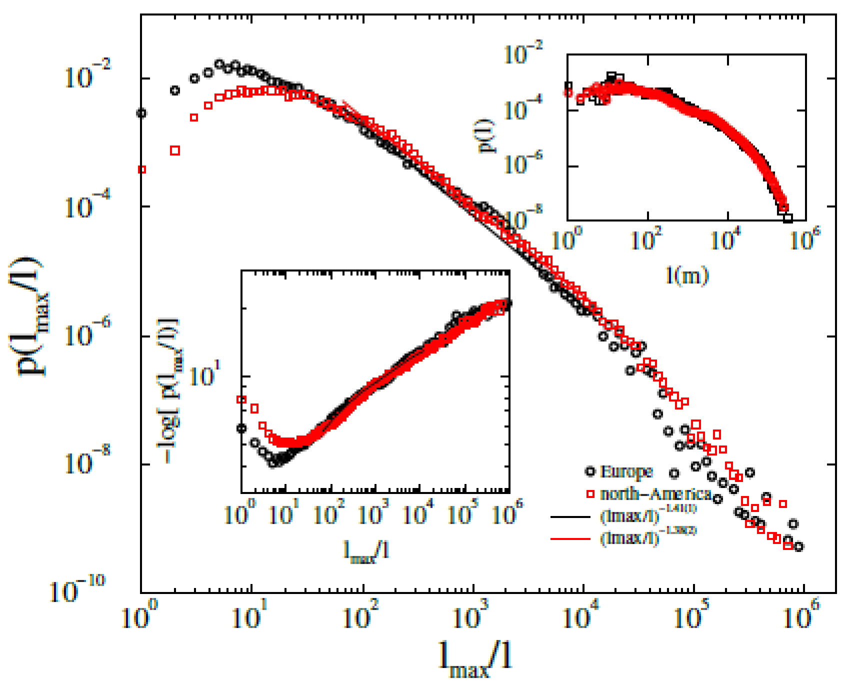

FIG. 14. Probability distributions of the inverse of cable lengths of the European and North-American SciGRID networks. Left inset: the same data plotted on the $-\ln(p)$ scale to compare with the stretched exponential assumption, that would correspond to a straight line tail, Right inset: probability distributions of the line lengths in meters.

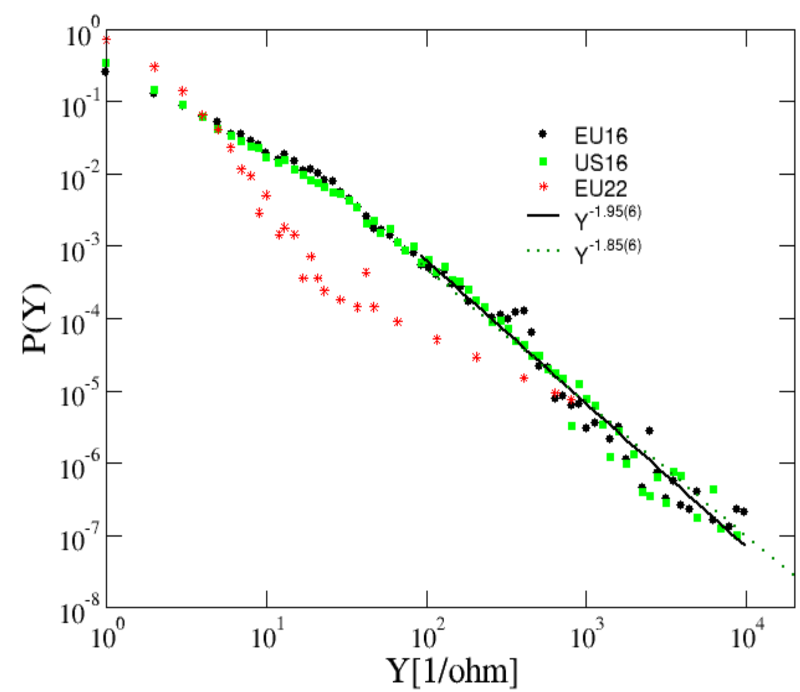

PL exponents ~ 2, **Universal ?**

Load and generator power distributions

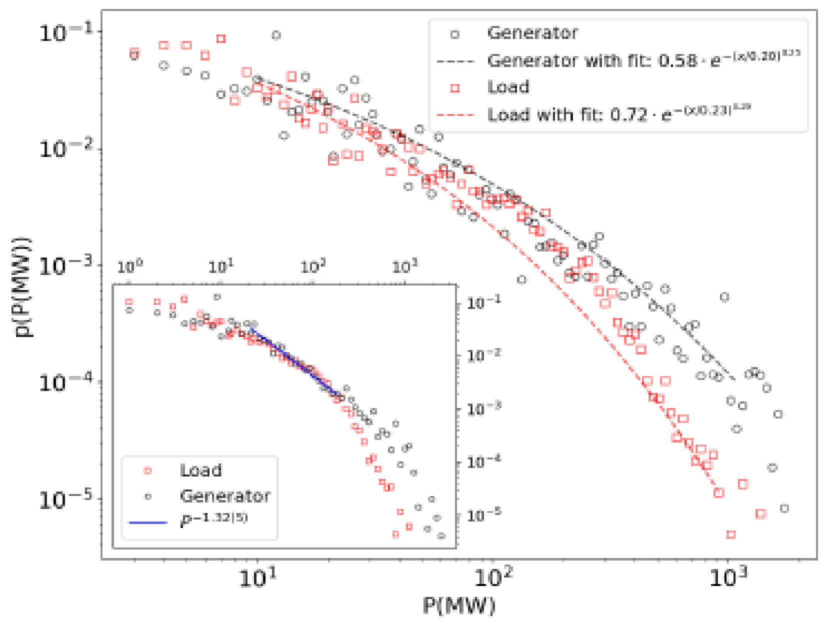

FIG. 5. Distribution of nodal generations and loads of the ENTSO-E 2016 database. Power-law fits were applied to the [20...300] MW range in the inset figure. The exponents of the fits are: $y = 1.16(5)$ both for generation and load curves, respectively. The load data shows an earlier size cutoff, which is an important characteristic of traditional power systems, where energy is produced in a centralized manner by large power plants to increase efficiency, and energy is consumed in a distributed manner. The main figure shows the same data, with stretched exponential fits, according to Eq. (7) in the range [10...1000] MW

$$p(k) \propto \exp(-(k/B)^{\beta})$$

Load and generator power distributions

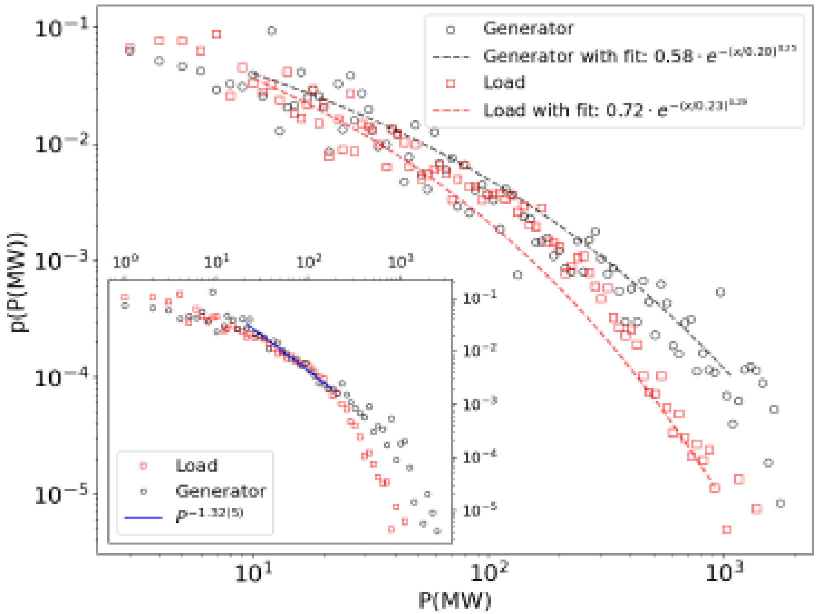

FIG. 5. Distribution of nodal generations and loads of the ENTSO-E 2016 database. Power-law fits were applied to the [20...300] MW range in the inset figure. The exponents of the fits are: $y = 1.16(5)$ both for generation and load curves, respectively. The load data shows an earlier size cutoff, which is an important characteristic of traditional power systems, where energy is produced in a centralized manner by large power plants to increase efficiency, and energy is consumed in a distributed manner. The main figure shows the same data, with stretched exponential fits, according to Eq. (7) in the range [10...1000] MW

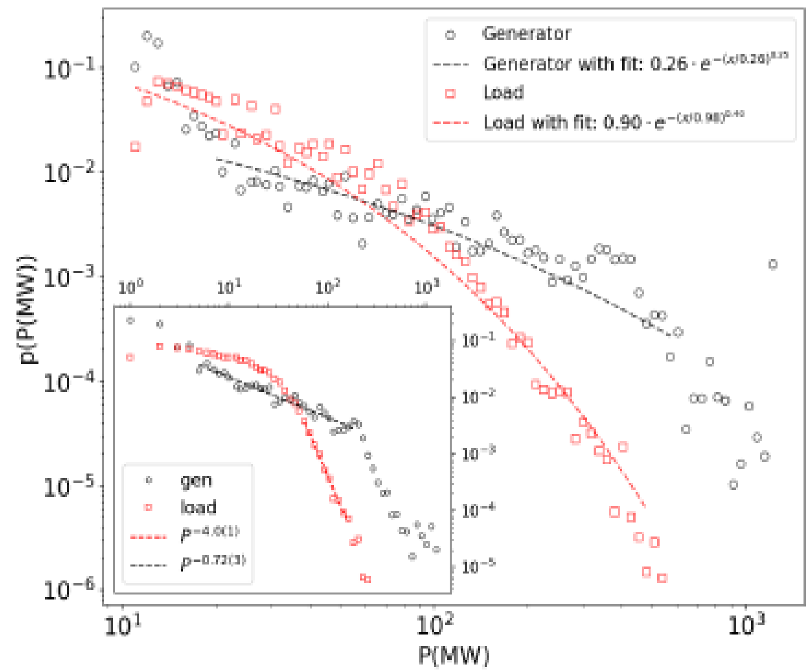

FIG. 6. Distribution of nodal generations and loads of the 2021 US [69] database. Inset: different power-law fits were applied to the [5...200] MW for generators and [50...200] MW for loads. The load data shows an earlier size cutoff as for the European case. The main figure shows the same data with stretched exponential fit according to Eq. (7) in the range [20...500] MW.

$$p(k) \propto \exp\left(-(k/B)^{\beta}\right)$$

Load and generator power distributions

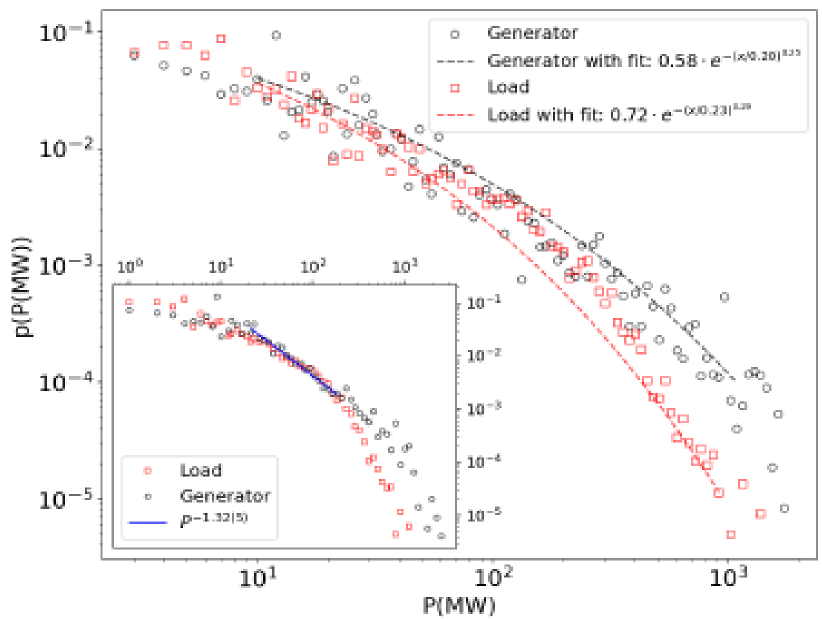

FIG. 5. Distribution of nodal generations and loads of the ENTSO-E 2016 database. Power-law fits were applied to the [20...300] MW range in the inset figure. The exponents of the fits are: $y = 1.16(5)$ both for generation and load curves, respectively. The load data shows an earlier size cutoff, which is an important characteristic of traditional power systems, where energy is produced in a centralized manner by large power plants to increase efficiency, and energy is consumed in a distributed manner. The main figure shows the same data, with stretched exponential fits, according to Eq. (7) in the range [10...1000] MW

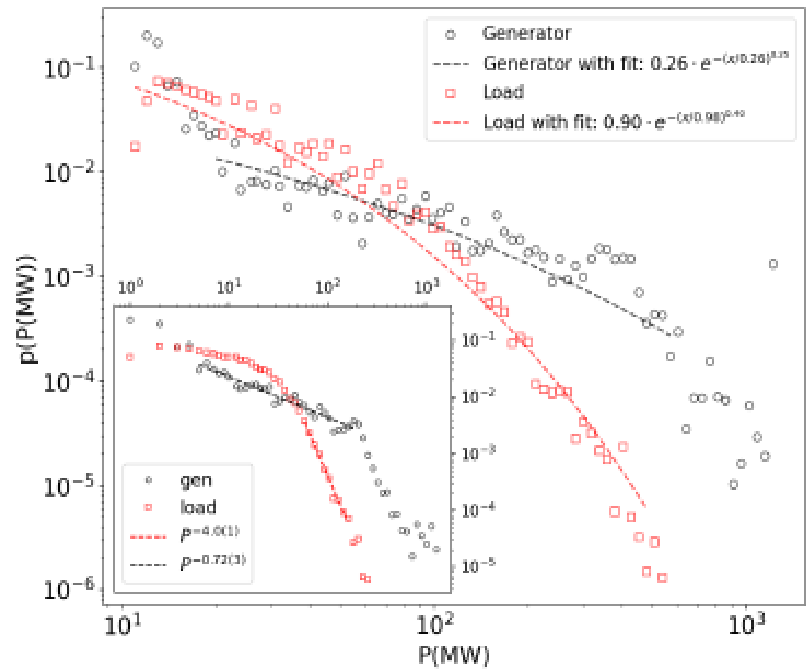

FIG. 6. Distribution of nodal generations and loads of the 2021 US [69] database. Inset: different power-law fits were applied to the [5...200] MW for generators and [50...200] MW for loads. The load data shows an earlier size cutoff as for the European case. The main figure shows the same data with stretched exponential fit according to Eq. (7) in the range [20...500] MW.

$$p(k) \propto \exp(-(k/B)^{\beta})$$

β ~ 0.25 Universal ?